Journal of Statistical Physics (2026) 193:64
https://doi.org/10.1007/s10955-026-03621-2

Wealth Thermalization Hypothesis and Social Networks

Klaus M. Frahm[1,2] · **Dima L. Shepelyansky**[1,2]

Received: 22 September 2025 / Accepted: 26 April 2026

Abstract
In 1955 Fermi, Pasta, Ulam and Tsingou performed first numerical studies with the aim to obtain the thermalization in a chain of nonlinear oscillators from dynamical equations of motion. This model happend to have several specific features and the dynamical thermalization was established only later in other studies. In this work we study more generic models based on Random Matrix Theory and social networks with a nonlinear perturbation leading to dynamical thermalization above a certain chaos border. These systems have two integrals of motion being total energy and norm so that the theoretical Rayleigh-Jeans thermal distribution depends on temperature and chemical potential. We introduce the wealth thermalization hypothesis according to which the society wealth is associated with energy in the Rayleigh-Jeans distribution. At relatively small values of total wealth or energy there is a formation of the Rayleigh-Jeans condensate, well studied in physical systems such as multimode optical fibers. This condensation leads to a huge fraction of poor households at low wealth and a small oligarchic fraction which monopolizes a dominant fraction of total wealth thus generating a strong inequality in human society. We show that this thermalization gives a good description of real data of Lorenz curves of US, UK, the whole world and capitalization of companies at Stock Exchange of New York SE (NYSE), London and Hong Kong. It is also shown that above a chaos border the dynamical Rayleigh-Jeans thermalization takes place also in social networks with the Lorenz curves being similar to those of wealth distribution in world countries. Possible actions for inequality reduction are briefly discussed.

1 Introduction

In 1872 Ludwig Boltzmann published the fundamental work [1] that became the foundation of the theory of statistical physics and thermalization emerging from the dynamical laws of time reversible classical motion of many-body systems. Of course, certain approximations

Communicated by Antonio Ponno.

These authors contributed equally to this work

✉ Klaus M. Frahm
klaus.frahm@utoulouse.fr

Dima L. Shepelyansky
dima@irsamc.ups-tlse.fr

1 Lab. Physique Théorique, Université Toulouse III - Paul Sabatier, UPS, CNRS, Toulouse, France

2 Univ Toulouse, CNRS, LPT,, Toulouse, France

Published online: 27 May 2026

had been used there, thus considering only pair collisions of gas particles. But this was only the first step in the demonstration that the statistical laws follow from the dynamical equations. One of the important results obtained in [1] was the Boltzmann H-theorem that a system entropy is monotonically growing with time or remains constant at the steady-state.

The first numerical experiment with the aim to directly obtain statistical thermalization from dynamical equations of motion was done by Fermi, Pasta, Ulam and Tsingou in 1955 studying the dynamics of a chain of nonlinear oscillators on the most powerful MANIAC I computer (at this time) with an expectation to obtain the thermal energy equipartition between oscillator modes [2]. However, opposite to expectations the conclusion of authors was that "The results show very little, if any, tendency toward equipartition of energy between the degrees of freedom." [2].

Several explanations had been proposed to explain this result. Zabusky argued in [3] that in the continuum limit the Fermi-Pasta-Ulam (FPU) problem is close to the Korteweg-de Vries equation with stable solitons shown to be completely integrable [4], as well as the nonlinear Schrödinger equation [5]. Also, at weak nonlinearity the FPU α-model is close to the completely integrable Toda lattice [6, 7]. Another explanation of absence of thermalization in the FPU problem was given in [8–10] showing that below a certain chaos border, determined by the strength of the nonlinear interactions between oscillators, the system is located in the regime of Kolmogorov-Arnold-Moser (KAM) integrability and only above this border an overlap of nonlinear resonances takes place with emergence of chaos and thermalization. Indeed, above a chaos border numerical simulations demonstrated an emergence of dynamical thermalization with energy equipartition as reported in [9, 10]. Possibilities of low energy chaos in the FPU model were discussed in [11],

It should be pointed out that while impressive mathematical results and theorems were obtained by mathematicians (see e.g. [12, 13] and Refs. therein) they remained usually not applicable to thermalization in physical nonlinear systems which usually have a divided phase space (see [14, 15]) where integrable islands of stable motion are often embedded in a chaotic component. Thus the KAM theorem is valid for unrealistically weak nonlinear perturbations [12, 13] and it is more appropriate to use the Chirikov criterion of overlapping resonances to estimate more realistic parameters for a chaos border [14, 15] (even if this criterion is not working for completely integrable systems like the Toda lattice for example).

An overview of the full richness of the FPU model and various regimes of its nonlinear dynamics has been presented 50 years after [2] in the book [16]. The variety of studies presented there clearly demonstrates that this model has an important role in the investigations of nonlinear dynamics. However, at the same time the variety of different features of FPU dynamics indicates that the FPU model does not belong to a class of generic oscillator systems with nonlinear interactions.

With the aim to capture the generic features of dynamical thermalization the nonlinear random matrix model (NLIRM) was proposed in the work [17], submitted 150 years after the Boltzmann article [1]. In this model, the linear unperturbed Hamiltonian is described by a random matrix that can be also viewed as a system of linear oscillators with complex linear couplings. The chaos in this system is induced only by a nonlinear perturbation that can be local or can have a certain interaction range. Thus in this model the unperturbed properties of eigenmodes and eigenenergies are described by the generic Random Matrix Theory invented by Wigner for a description of the spectra of complex nuclei, atoms, and molecules in many-body quantum mechanics [18]. Indeed, RMT finds a variety of applications in multiple areas of physics [19, 20] including systems of quantum chaos where the dynamics is chaotic in the classical limit [21, 22].

In [17] it was shown that above a certain chaos border the dynamical thermalization takes place leading to the Rayleigh-Jeans thermal distribution (see Eq. (2.1 below) well known in classical thermodynamics [23, 24]. However, the dynamics of the NLIRM system has two integrals of motion being the total energy and norm (or probability that is very natural for quantum evolution). Due to this the Rayleigh-Jeans distribution is characterized by temperature and chemical potential. Such a situation appears in various classical systems including dynamics of nonlinear waves (see e.g. [25]). In fact this type of thermal distribution was described and experimentally observed for light propagation in multimode optical fibers (see e.g. review [26] and Refs. below). The important feature of the Rayleigh-Jeans thermalization is the condensation of a main fraction of system norm or probability at the lowest energy modes of the system. However, in [26] the emergence of such thermalization and condensation was attributed to the turbulence like energy flows similar to those of the Kolmogorov-Zakharov turbulence spectra of nonlinear waves [25] (even if it is stated [26] that the dynamics is Hamiltonian). In contrast, it is argued in [17, 27] that such Rayleigh-Jeans thermalization and condensation appear due to dynamical chaos emerging above a chaos border while below this border the thermalization is absent and the system is located in the integrable KAM regime. Certain similarities of this condensation with the Fröhlich condensate proposed for molecular systems at room temperature [28, 29] are discussed in [27]. The striking applications of Rayleigh-Jeans thermalization are discussed in this work.

This work is composed of two parts. In the first Part I, we push forward the Wealth Thermalization Hypothesis according to which the wealth is associated with system energy and the wealth distribution in the human society is described by the Rayleigh-Jeans thermalization and condensation which are at the origin of strong inequality in the world. The comparison of the obtained thermalization results with the real data of wealth inequality in countries and stock exchange markets confirms the validity of the Rayleigh-Jeans thermal description. In the second Part II, we provide certain additional arguments and justifications for this hypothesis. In particular, we argue that social networks, actively investigated in the network science and society (see e.g. books [30, 31]), provide a reliable model of social relations in the society. While the previous studies of social networks describe the social relations and links only in the frame work of linear matrix algebra we introduce a nonlinear interaction in such social networks. Similarly to the NLIRM results [17] our studies show that above a certain chaos border for the strength of the nonlinearity dynamical thermalization takes place in social networks being well described by the steady-state Rayleigh-Jeans distribution. This gives an additional support to the Wealth Thermalization Hypothesis. In this way the problem of emergence of statistical laws from dynamical equations of motion finds new application perspectives.

We note that various properties of the dynamical Rayleigh-Jeans thermalization and condensation were discussed in [17, 27, 32, 33] and an interested reader can find them there. Additional results for real data for wealth inequality can be found in [32, 33] with their Rayleigh-Jeans thermodynamic description.

We also point out that the statistical phenomena similar to the Rayleigh-Jeans condensation, called constraint-driven condensation [34], were studied in [34–36] showing the existence of different aggregation phases for continuous systems. In the systems we study here we have only a discrete number of system states (e.g. energies) and due to that we do not enter in the discussion of phase transitions for such discrete systems. Indeed, all data for wealth inequality, available to us, contain at maximum about 2600 states (companies at a stock exchange). It is possible that for wealth inequality of countries or the whole world the continuum regime can be considered but this data are not publicly available. Hence, for the discrete systems with available data, we discuss the fractions of population (households or

companies) that are very poor or very rich compounding to the phases of poor and oligarchic phases. The constraint-driven condensation is a generic phenomenon and it finds applications in diverse physical systems such as coalescence in granular media, jamming in traffic, gelation in networks [34] and financial data analysis [36]. Here we discuss a new application of such type of phenomenon for social systems showing that it describes the wealth inequality in the world.

The main results of this research are presented in Sect. 2 (Part I) for links between wealth inequality and Rayleigh-Jeans thermalization and in Section 3 (Part II) for dynamical thermalization in social networks supporting the Wealth Thermalization Hypothesis discussed in Part I.

2 Part I: Wealth Thermalization Hypothesis

2.1 Prologue I

The wealth distribution in the human society is characterized by a striking inequality (see e.g. [37–39]). Thus for the whole world 50% of the population owns only 2% of total wealth, while 10% of population owns 75% of total wealth and 1% of population owns 38% of total wealth [38].

The distribution of wealth is usually described by the Lorenz curve [39, 40] which gives the dependence of accumulated normalized wealth $0 \leq w \leq 1$ on the cumulated normalized fraction of population or households $0 \leq h \leq 1$. Thus the equipartition of wealth corresponds to the diagonal $w = h$ and the doubled area between diagonal and the Lorenz curve $w(h)$ determines the Gini coefficient $0 \leq G \leq 1$ [39, 41]. Values of G can be found in [42] for world countries in 2021 being in the range $0.59 < G < 0.90$; for the whole world $G = 0.889$.

The sharing of wealth varies from country to country but the global features remain rather similar with a big fraction of very poor population with scanty wealth and a very small fraction of rich people having a significant fraction of a country's total wealth. This gives an insight that some fundamental underground reasons can be at the origin of this inequality.

Diverse methods of statistical mechanics and physical kinetics [23, 24, 43] have been proposed and used by different research groups [44–52]. Various models of interacting agents are investigated including Random Asset Exchange models [44–52]. In several of these models there is appearance of some kind of oligarchic phase with a significant wealth accumulation by a group of agents [47, 50–52]. The specific arguments are presented in a favor of the Boltzmann-Gibbs type description of distribution of money, wealth and income [46, 48]. Also a nonlinear Fokker–Planck description of asset exchange is proposed [50, 51] with emergence of oligarchic phase. A few important elements are stressed in [50, 51]: the conservation of two integrals of system evolution being the total wealth and total norm (or number of agents), the argument in favor of consideration of wealth instead of money based on the small-transaction approximation. The conservation of two integrals is rather natural assumption since a Gross domestic product and population of a country or the whole world are only weakly changed on a typical time scale of one year.

The above models give interesting insights for understanding of certain features of wealth distribution in the world countries but they remain model specific and their universality remains questionable. The universality of the Boltzmann-Gibbs thermal distribution is the ground element of the approach developed in [46, 48] but it does not capture emergence of a huge condensate of poverty in various countries.

Our studies here are based on the Wealth Thermalization Hypothesis (WTH) according to which the wealth of a country is described by the Rayleigh-Jeans (RJ) thermal distribution:

$$\rho_m = \frac{T}{E_m - \mu} \text{ (RJ)}. \tag{2.1}$$

Here we assume that the system wealth has certain states $0 \leq m < N$ with energies E_m and the population probabilities in these states are ρ_m. Thus a system wealth is associated with a system energy. Also in (2.1) the parameters T and $\mu(T)$ are the system temperature and its chemical potential dependent on T. As in [50] there are two conserved integrals of motion being the total norm of population, fixed to be unity for convenience, $\sum_m \rho_m = 1$, and the system average wealth being its total energy $\sum_m E_m \rho_m = E$. For a given system energy E and unity norm these two integrals of motion determine the system temperature T and its chemical potential $\mu(T)$. The von Neumann entropy S of the system is determined by the usual relation [23, 24]: $S = -\sum_m \rho_m \ln \rho_m$ with the implicit theoretical dependencies on temperature $E(T)$, $S(T)$, $\mu(T)$. Here ρ_m play the role of occupation probabilities for the oscillator modes E_m similarly as in a discrete quantum system. However, for a classical system with a continuous probability density of the classical oscillator variables the entropy has to be computed using this continuous probability density and for the RJ-distribution here one can show that this gives the Boltzmann entropy $S_B = \sum_m \ln \rho_m + const$ which satisfies the standard thermodynamic relation $dS_B/dE = 1/T$ (see discussion below in Section 3.3 for more details on this) [23, 24].

The RJ thermalization (2.1) is universal and describes a variety of classical systems [23, 24] including nonlinear waves [25], light propagation in multimode optical fibers with a nonlinear media [53–58], dynamical thermalization for nonlinear perturbation of the Random Matrix Theory (RMT) [17] and the nonlinear Schrödinger equation (NSE) in quantum chaos billiards [27]. It is pointed out in [18–20] that RMT finds a variety of applications in multiple areas of physics including nuclei, complex atoms and systems of quantum chaos whose dynamics is chaotic in the classical limit. Thus almost any physical nonlinear interaction above a chaos border [17] leads to dynamical RJ thermalization (2.1). An example of such a system can be an ensemble of N nonlinear RMT oscillators with random frequencies $\omega_m \propto E_m$ of an ensemble of N agents with nonlinear interactions leading to the RJ thermalization (2.1). The thermalization can have a dynamical origin when chaotic nonlinear dynamics leads to (2.1) or it can appear due to an external thermal bath. We suppose that for WTH a dynamical origin is more adequate since in a first approximation on a scale of one year a country or the whole world can be considered to be quasi-isolated from slow external processes.

Due to the presence of two integrals of motion, energy and norm, RJ thermalization has the phase of RJ condensate emerging at relatively low total energy E or low temperature T [27, 54, 55]. Thus at low energy and a large number of oscillators, as in [17], or a large number of interacting agents, the fraction of RJ condensate is approaching unity being concentrated at a vicinity of the ground state energy E_0 being zero or very close to zero [27]. Thus the RJ condensate (2.1) very naturally has a huge fraction of very poor agents that naturally describes the huge world wealth inequality where 50% of population owns only 2% of the total wealth [38]. Below we describe in detail various consequences of WTH (2.1) and compare the results of this theory with real Lorenz curves of certain countries and the whole world.

2.2 RJ thermalization and condensation

We start from a model with N equidistant energy levels $0 \leq E_m = m/N \leq B$ located in the energy band of total width B. This corresponds to certain levels of wealth for N agents

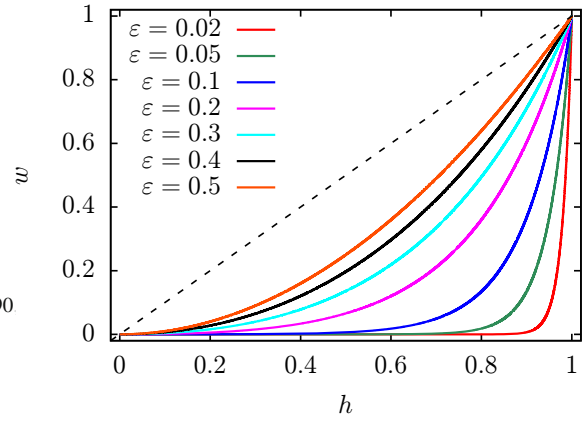

Fig. 1 Lorenz curves for the RJS model with the linear spectrum $E_m = m/N$ (for $N = 10000$) for different values of the rescaled energy $\varepsilon = E/B$. The x-axis corresponds to the cumulated fraction of households (h) and the y-axis to the cumulated fraction of wealth (w). The dashed line is the line of perfect equipartition $w = h$. The Gini coefficients G for all curves are $G = 0.9600,\ 0.9000,\ 0.8006,\ 0.6250,\ 0.4990$ (bottom to top)

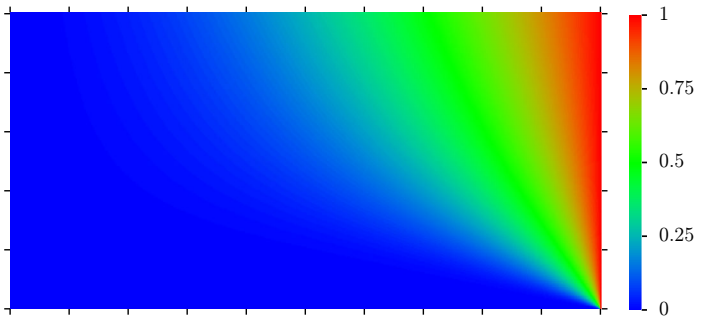

Fig. 2 Color plot of wealth w from Lorenz curves of the RJS model ($N = 10000$). The x-axis corresponds to the fraction of households $h \in [0, 1]$ and the y-axis to the rescaled energy $\varepsilon = E/B \in [0, 0.5]$. The ticks mark integer multiples of 0.1 for h and ε

with a fraction of agents on level m being ρ_m. The conserved average system energy is $E = \sum_m E_m \rho_m$ and the dimensionless parameter $\varepsilon = E/B$ determines its fraction with respect to the maximal system energy B. We call this model the RJ standard (RJS) model. On the basis of WTH with RJ distribution (2.1) the local (normalized) wealth on level i is $(E_i/E)\rho_i$ and the cumulated wealth on levels $[0, m]$ is $w = \sum_{i=0}^{m} (E_i/E)\rho_i$ with the cumulated fraction of population or households $h = \sum_{i=0}^{m} \rho_i$. Computing both sums for all values of $m = 0, 1, \ldots$ provides the Lorenz curve $w(h)$.

Since the Lorenz curve describes the normalized distribution of cumulated fractions of wealth $w \in [0, 1]$ and households $h \in [0, 1]$ we use the ratio E_i/E (since $E = \sum_i E_i \rho_i$) in the definition of wealth ensuring that $w = 1$ at $h = 1$ for the total population. At given ε the relation (2.1) and two integrals of energy and norm determine the physical parameters T, μ, S. In our numerical studies we use $N = 10000$ which practically corresponds to the continuous limit with results independent of N. The typical dependencies of T and μ on ε in the RMT and RJS models are given in Refs. [17, 27]. As discussed in [17, 27] for $\varepsilon > 1/2$ the temperature T becomes negative and at ε close to unity there is a formation of an RJ condensate on highest energy levels with $E_m \to B$. Many unusual properties of RJ thermalization have been discussed in [17, 27, 32]. Even if the regime with negative temperatures has been realized in fiber experiments [53, 58] we consider that such a regime is not applicable to human society and hence we consider only the range with $0 \le \varepsilon \le 1/2$.

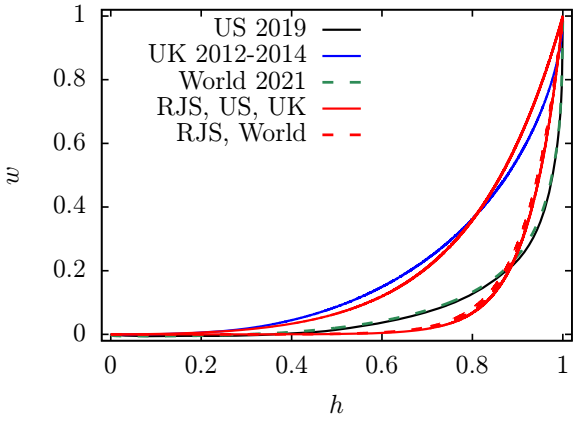

Fig. 3 Comparison of the Lorenz curves for US 2019 (black), UK 2012-2014 (blue), World 2021 (dashed green) with those of RJS model (red curves; $N = 10000$); US and World curves are rather close. For the three referenced curves Gini coefficients are $G = 0.852, 0.626, G = 0.842$ respectively and the rescaled energies $\varepsilon = E/B$ of the RJS model are respectively fixed as $\varepsilon = 0.07420$, $\varepsilon = 0.1996$, $\varepsilon = 0.07911$ so that the corresponding Gini coefficients match the referenced data

The Lorenz curves for the RJS model at several ε values are shown in Fig. 1. We remind that the Gini coefficient G is defined as the doubled area between the Lorenz curve and the diagonal $w = h$ with $G = 0$. Due to the RJ condensate there is a very high fraction of poor households f_p (with $w \leq 0.02$) and a small fraction of rich ones f_r (with $w \geq 0.75$) who owns a huge fraction of total wealth. Thus the RJS model naturally describes the big phase of poor households and the oligarchic phase of small fraction of households capturing the big fraction of total wealth. At maximal $\varepsilon = 0.5$ with ($\mu \to -\infty$) all ρ_m are equal and hence the Lorenz curve is $w = h^2$ with the limiting minimal Gini coefficient $G = 1/3$ for the RJS model. The dependence of cumulated wealth w on h and ε is shown in Fig. 2. It clearly shows the phase of poor households (blue), corresponding to the RJ condensate, and the oligarchic phase of very rich households (red). Thus we see that the RJ thermal distribution (2.1) describes the main qualitative features of wealth inequality of human society [38].

From Figs. 1, 2 we see that for the RJS model the WTH based on (2.1) captures main elements of wealth inequality but it is important to see if it can reproduce the real Lorenz curves for the whole world and specific countries. For this comparison of WTH theory we choose three cases with the Lorenz curves for: the whole world from [38] (integration of front page data gives cumulative w, h values); USA 2019 case from [59] and UK 2012-2014 case from [60]. These real Lorenz curves are compared with those obtained from the RJS model (2.1) in Fig. 3. For the comparison values of ε are fixed in such a way that Gini coefficient is the same for theory and real data curves. The comparison for UK case shows that there is a good agreement of real and theoretical Lorenz curves even if there is a certain difference for the range $0.9 \leq h \leq 1$. The difference is more visible for USA case and the whole world (Lorenz curves are very similar for these two cases). We also find that the RJS Lorenz curves have a satisfactory agreement with the Lorenz curves for France and Germany (see [32]; data are obtained for the year 2010 from [61]).

In view of certain differences between real Lorenz curves and those obtained from RJS model (see Fig. 3) we also study the case of RJ distribution (2.1) with level energies E_m taken from a random matrix of size $N = 1000$ as it was discussed in [17]. For this RJ RMT model the density of states is $\nu = dm/dE_m = \frac{2N}{\pi}\sqrt{1 - E^2}$ with typical eigenvalues in the interval $E_m \in [-1, 1]$ and we shift all E_m to $E_m - E_0$ to have nonnegative values $E_m \geq 0$ in (2.1). The comparison of Lorenz curves for US and UK cases with the results of the RJ RMT model is shown in Fig. 4a. The similarity between real and RMT model data is a bit less good then those in Fig. 3 for the RJS model. This shows that the density of states ν can affect the Lorenz curves. Indeed, we have $\nu = \text{const.}$ for the RJS model being different from the semi-circle law of RMT model.

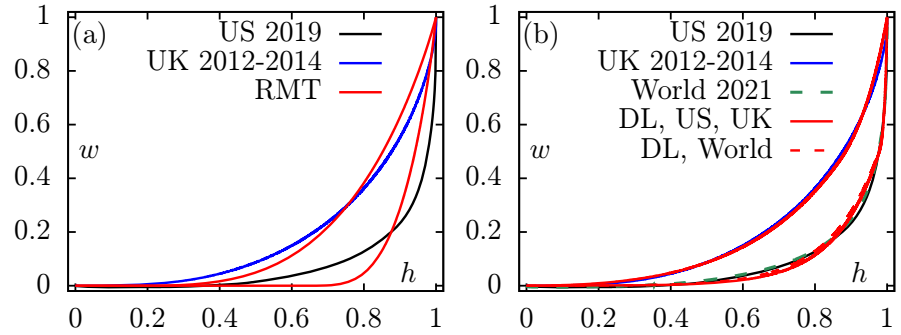

Fig. 4 Both panels compare the Lorenz curves for different data sets (black for US 2019, blue for UK 2012-2014 and green dashed for World 2021) with those of the RMT model (a) and the DL model (b). As in Fig. 3 the Gini coefficients G of the reference curves are used to fix the rescaled energy $\varepsilon = E/B$ of the corresponding model such that the model curves (red) have the same G. For the RMT model (a) only two data sets are shown $\varepsilon = 0.07996$ (US) and $\varepsilon = 0.2027$ (UK). For the DL model (b) the parameter values are $a = 16$ (US and World) and $a = 3$ (UK). These values are fixed to have a best possible fit of the model data with those of the reference curves. The chosen values $\varepsilon = 0.01434$ (US), $\varepsilon = 0.1355$ (UK), $\varepsilon = 0.01535$ (World) match the G values of the reference data. In (b) the curves for US and World are rather close. In (a) the RMT Lorenz curves are shown for one realization of a random matrix, other realizations give practically the same curves

To reproduce the real Lorentz curves from [38, 59, 60] in a better way we also analyze a double-linear (DL) model with energies $E_m = m/N$ for $m < N/2$ and $E_m = E_{N/2} + a(m - N/2)/N$ for $m \geq N/2$ at $N = 10000$ with $a = 16$ ($B = 8.5$) for US and World data, and $a = 3$ ($B = 2$) for UK data. In this type of model the density of states takes not one but two values being $\nu = 1$ and $\nu = 1/a$. The existence of two ν values can correspond to a society where high wealth energy E_m values are only accessible to very rich people whose density is lower compared to common people. The comparison of real Lorenz curves with those of the DL model is shown in Fig. 4b demonstrating a better proximity between real Lorenz curves and those from the DL model as compared to the results of the RJS model in Fig. 3. However, the DL model has two fit parameters a, ε while the RJS model has only one ε.

We also remind that for the RJS model the minimal Gini value is $G = 1/3$ that is reached at maximal physical value of $\varepsilon = 1/2$. Thus to have $G < 1/3$, we need to significantly modify the density of states ν. Indeed, we can obtain a perfect complete wealth and energy equipartition with $w = h$ and $G = 0$ for the case when all $E_m = E_0$ values are the same. In this case, the integrals of energy and norm give only one conservation law and all states have the same energy and same population. A small spectrum modification to $E_m = E_0 + m/N$ with a constant energy offset E_0 leads to Lorenz curves being closer to the diagonal with small Gini values $G < 1/3$ and a finite slope $w(h) \approx [E_0/(\varepsilon + E_0)]\, h$ at small h. We call this model the equipartition (EQI) model.

The dependence of the Gini coefficient G on ε is given in Fig. 5 for the different models. In global the results show that an increase of ϵ leads to a reduction of G. Also in Fig. 6, we show the dependence of fractions of poor f_p and rich oligarchic f_r households on ε for the RJS model. Thus at $\varepsilon = 0.07$ we have $f_p = 0.73$ and $f_r = 0.097$ that is close to the real values $f_p = 0.53$(US), 0.5(World) and $f_r = 0.09$(US), 0.1 (World) while for UK we have $f_p = 0.32$, $f_r = 0.28$ corresponding to a higher $\varepsilon \approx 0.21$. Furthermore Fig. 6 shows that the fraction of poor households can be significantly reduced and the fraction of rich households can be increased by increasing parameter ε, thus diluting the oligarchic phase.

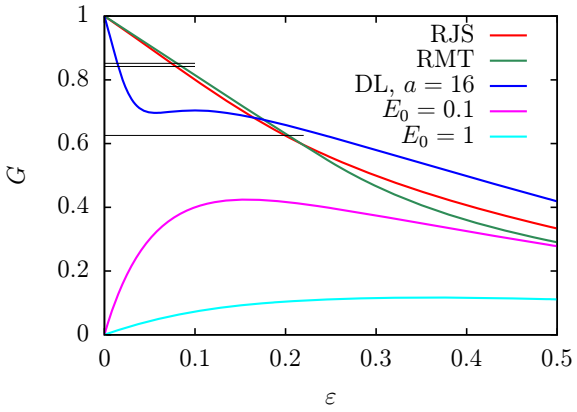

Fig. 5 Gini coefficient versus rescaled energy $\varepsilon = (E - E_0)/(E_{N-1} - E_0)$ for the RJS model (red), RMT model (green), DL model (blue; only for the case $a = 16$), and the EQI model (pink for the offset $E_0 = 0.1$ and cyan for $E_0 = 1$). The thin black lines show the values of $G = 0.852$, $G = 0.842$ and 0.626 for the data of US 2019, World 2021 and UK 2014. The intersection of these lines with the red and green curves correspond to ε values used in Figs. 3, 4

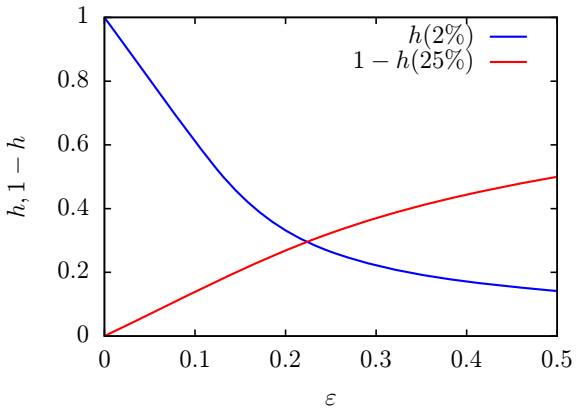

Fig. 6 Dependence of fraction of poor households $f_p = h(2\%)$ (owning 2% of wealth) and fraction of rich oligarchic households $f_r = 1 - h(25\%)$ (owning 75% of wealth) on the rescaled energy $\varepsilon = E/B$ for the RJS model

Finally, we mention that for the RJS model it is possible to work out analytic expressions (at $N \to \infty$) for the Lorenz curve and other quantities that accurately match the numerical data (see [32]). These expressions depend on μ and at small $\varepsilon \leq 0.2$ (with $\mu \approx 0$), we have $w(h) \approx e^{(h-1)/\varepsilon}$ and $G \approx 1 - 2\varepsilon$, matching 3 values of G in Fig. 1.

2.3 RJ thermalization and universality

Above we presented the comparison of real Lorenz curves of countries and the whole world with the theoretical results of the RJS model based on the physical phenomenon of RJ thermalization and condensation. Since this thermalization is universal for classical systems when the norm and energy are conserved we expect that other systems will be also describe by the RJS model and its extensions.

To check this expectation we analyze the capitalization data for S&P500 companies at the New York Stock Exchange (NYSE), companies of London stock exchange and Hong Kong stock exchange. The data are obtained from the open public sources [62], [63] and [64] respectively. From these sources we construct the real Lorenz curves and compare them with those given by the RJS model for these three cases (see [32]). The comparison shows that the RJS model qualitatively describes the real Lorenz curves behavior approximately with the same level of agreement as it was for countries and the whole world cases considered before.

To obtain an RJ extended (RJE) model giving a better agreement with the real Lorenz curves for countries and stocks exchange we make the following extension of the RJS model.

The comparison of the different data with the RJS model shows that typically the curves of the RJS model have a slower (final) growth rate. Since the latter is proportional to the energy E_m one could try an extended model where the energy values grow stronger with m. One step in this direction is the DL model which allowed for a considerable improvement as can be seen in the right panel of Fig. 4. Another possibility is to choose an exponential growth of E_m but in such a way that still $E_m \sim m$ for small m. This can be achieved by the formula

$$E_m = \frac{\exp(a\,(m/N)) - 1}{a} \tag{2.2}$$

which we call RJE model (RJ extended or RJ exponential model). Here a is an additional parameter of the model in addition to the value of ε which is now $\varepsilon = E/B$ with bandwidth $B = E_{N-1} \approx (e^a - 1)/a$. In the limit $a \to 0$, we recover simply the RJS model while with increasing values of a the exponential growth of E_m becomes more dominant.

The energy spectrum (2.2) corresponds to a density of states:

$$\nu(E_m) = \frac{dm}{dE_m} = \frac{d}{dE_m}\left(\frac{N\ln(1+aE_m)}{a}\right) = \frac{N}{1+aE_m} \tag{2.3}$$

which interpolates between a constant density of states $\nu(E_m) \approx N$ for $E_m \ll a^{-1}$ (as in the RJS model) and a power law decay $\nu(E_m) \approx N/aE_m \sim 1/E_m$ for $E_m \gg a^{-1}$.

To determine optimal values for the parameter a, we compute a reconstructed spectrum from a given Lorenz curve of some given data set. For this, we use an interpolated smooth expression of $w(h)$ for this data set which allows to compute the derivative $w'(h)$ at each value of h. Then for a given value of N (e.g. $N = 10000$), an initial guess of μ and the average energy value E (which is simply fixed by $E = 1$ to provide a certain energy scale since Lorenz curves are invariant with respect to the global energy scale), we compute a virtual spectrum E_m starting with its last value $E_N \approx w'(h_N = 1)$. Using the standard RJ expression for ρ_m (in terms of μ, E, E_m and $T = (E-\mu)/N$) we compute the associated value of ρ_N for E_N which allows to compute a reduced household value $h_{N-1} = h_N - \rho_N$ (with the initial boundary value $h_N = 1$). Then we use h_{N-1} to compute $E_{N-1} = w'(h_{N-1})$ which allows to obtain ρ_{N-1}, then h_{N-2} etc. This gives a recursion for E_m and h_m with decreasing values of m where the last value h_0 is a function of the initial guess of μ which is then modified/refined to ensure the boundary condition $h_0(\mu) = 0$ (by a suitable numerical iterative method to determine the zero of the function $h_0(\mu)$). The procedure is very sensitive to the quality of interpolation of $w(h)$ and of the initial data. Also the issue to determine a good value of μ is quite subtle with a certain number of technical complications. More details of this procedure can be found in [32] with one example figure for a reconstructed spectrum.

Using this reconstructed spectrum, we apply the fit to the function $E_m \approx C(e^{a\,(m/N)}-1)/a$ with two parameters C and a. The 2nd parameter C has no importance since one could apply an arbitrary fixed factor on (2.2) without changing the resulting Lorenz curve of the RJE model. This is because the construction procedure of Lorenz curve involves only the ratio E_m/E (with E being the average energy) so that the global energy scale (or bandwidth B) drops out.

To fix some procedure, we perform the fit of the reconstructed spectrum for two fit intervals for the rescaled level number $x = m/N$ being either $x \in [0, 0.7]$ or $x \in [0, 0.9]$ and select the resulting value of a for which the RJE model provides a closer Lorenz curve to the given

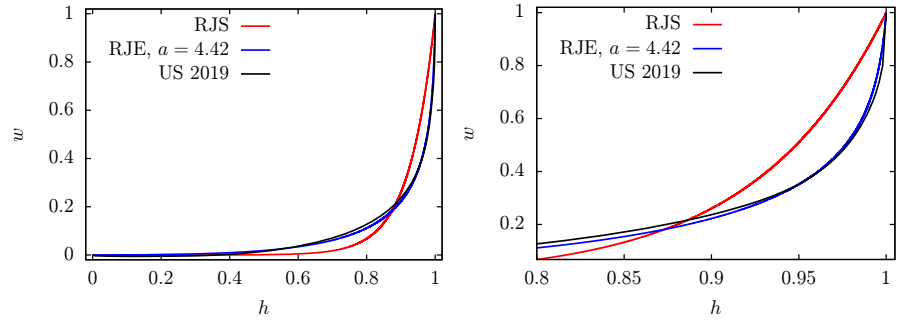

Fig. 7 Comparison of the Lorenz curve for the data of US 2019 (black) with the corresponding curves for the RJS model (red curve; $N = 10000$) and the RJE model with $a = 4.42$ (blue curve; $N = 10000$). The rescaled energy values $\varepsilon = 0.01233$ (RJE) and $\varepsilon = 0.07420$ (RJS) are obtained by matching the Gini coefficient $G = 0.8515$. The value of a is obtained by a fit from the reconstructed spectrum. The left (right) panel shows the full range $h \in [0, 1]$ (zoomed range $h \in [0.8, 1]$)

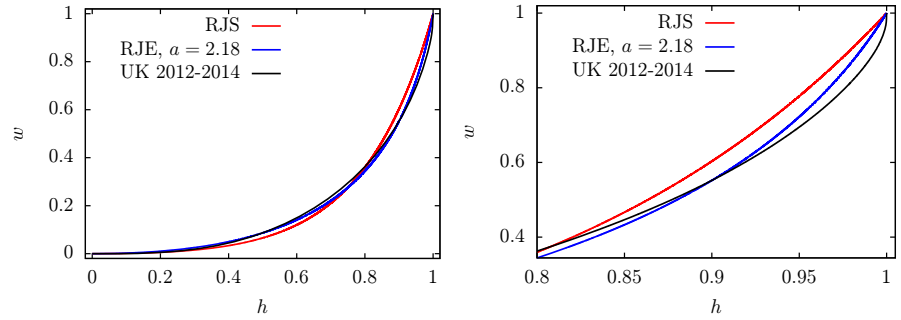

Fig. 8 Comparison of the Lorenz curve for the data of UK 2012-2014 (black) with the corresponding curves for the RJS model (red curve; $N = 10000$) and the RJE model with $a = 2.18$ (blue curve; $N = 10000$). The rescaled energy values $\varepsilon = 0.1332$ (RJE) and $\varepsilon = 0.1996$ (RJS) are obtained by matching the Gini coefficient $G = 0.6255$. The value of a is obtained by a fit from the reconstructed spectrum. The left (right) panel shows the full range $h \in [0, 1]$ (zoomed range $h \in [0.8, 1]$)

data set. In certain cases, the shorter fit interval provides a better fit value of a (cases where the global fit is of reduced quality for small x) and in other cases the longer fit interval is more accurate (cases where the global fit is also of rather good quality for small x).

The results for US 2019, UK 2012-2014, World 2010, FTSE 2024 (London stock exchange) and the Hong Kong 2025 stock exchange are shown in Figs. 7, 8, 9, 10 —11, in each case with two panels, top for the full range of $h \in [0, 1]$ and bottom for the zoomed range $h \in [0.8, 1]$. Here, we choose for simplicity the value of $N = 10000$ for the curves of both RJE and RJS models (the RJS curves are also shown for comparison). Other values such as $N = 1000$ or the given size of the data set, give the same Lorenz curves at graphical precision.

In all cases, the agreement of the RJE model with the data is significantly better than the RJS model. In particular for HK 2025, the agreement is close to perfect and even in the zoomed panel it is difficult to distinguish the theoretical RJE curve (blue) from the data (black). For the case UK 2012-2014 the original simpler RJS model was already quite good, but also here the RJE model provides a significant improvement. The RJE curves for US 2019 and World 2021 are also very good, nearly as good as the curve for HK 2025. For FTSE 2024

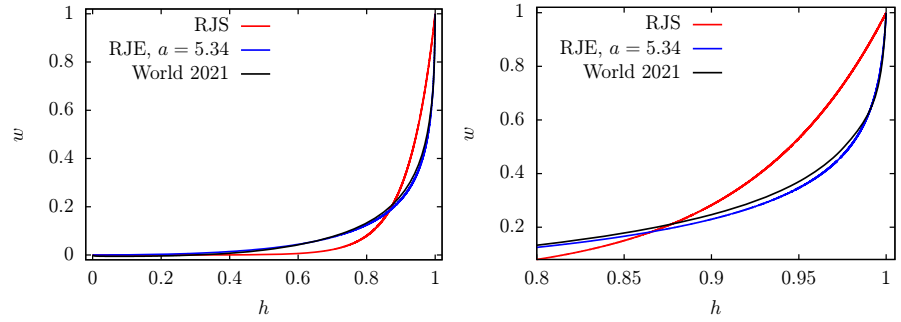

Fig. 9 Comparison of the Lorenz curve for the data of World 2021 from [38] (black) with the corresponding curves for the RJS model (red curve; $N = 10000$) and the RJE model (2.2) with $a = 5.34$ (blue curve; $N = 10000$). The rescaled energy values $\varepsilon = 0.008553$ (RJE) and $\varepsilon = 0.07911$ (RJS) are obtained by matching the Gini coefficient $G = 0.8420$. The value of a is obtained by a fit from the reconstructed spectrum. The left (right) panel shows the full range $h \in [0, 1]$ (zoomed range $h \in [0.8, 1]$)

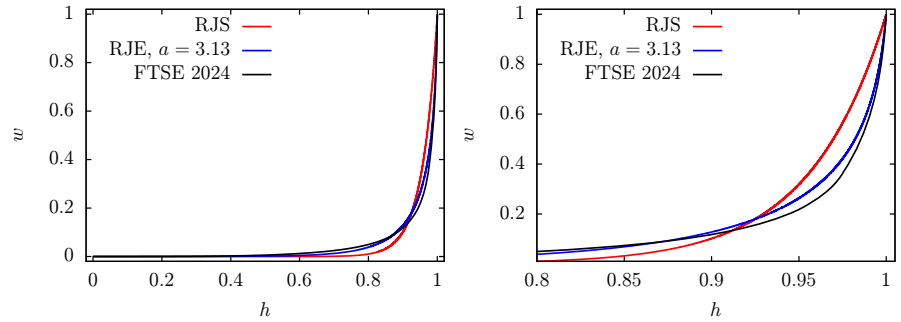

Fig. 10 Comparison of the Lorenz curve for the data of the London stock exchange FTSE at 31 December 2024 (black; data from Ref. [63]) with the corresponding curves for the RJS model (red curve; $N = 10000$) and the RJE model with $a = 3.13$ (blue curve; $N = 10000$). The rescaled energy values $\varepsilon = 0.01346$ (RJE) and $\varepsilon = 0.04376$ (RJS) are obtained by matching the Gini coefficient $G = 0.9126$. The value of a is obtained by a fit from the reconstructed spectrum. The left (right) panel shows the full range $h \in [0, 1]$ (zoomed range $h \in [0.8, 1]$)

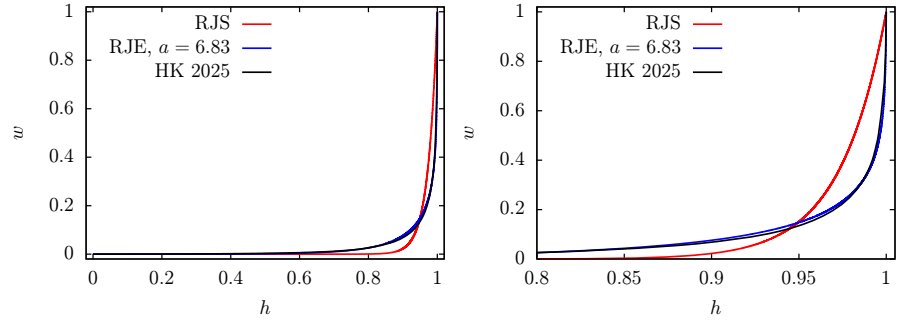

Fig. 11 Comparison of the Lorenz curve for the data of the Hong Kong stock exchange at 19 June 2025 (black; data from Ref. [64]) with the corresponding curves for the RJS model (red curve; $N = 10000$) and the RJE model with $a = 6.83$ (blue curve; $N = 10000$). The rescaled energy values $\varepsilon = 0.0008381$ (RJE) and $\varepsilon = 0.02648$ (RJS) are obtained by matching the Gini coefficient $G = 0.9471$. The value of a is obtained by a fit from the reconstructed spectrum. The left (right) panel shows the full range $h \in [0, 1]$ (zoomed range $h \in [0.8, 1]$)

the agreement of the data with the RJE model is a bit less perfect (since S&P500 captures only about 80% of NYSE) but still clearly better than the RJS model.

We also verified that for three other cases DE 2010, FR 2010 and NYSE 2025 the RJE model gives a good description with values $a = 4.2$, $a = 3.82$ and $a = 2.66$ respectively. Here the results have also a strongly improved agreement of the RJE model with the real data. For NYSE 2025 the agreement is slightly less good compared to other cases (since S&P sector captures only about 80 percent of total NYSE) but even here the RJE model is significantly better than the simple RJS model.

On the basis of presented results we conclude that the RJ thermalization gives a universal description of inequality described by the Lorenz curves for countries and company capitalization at stock exchange.

2.4 Overview of wealth thermalization results

In this Part I we use the WTH approach (2.1) to describe the wealth distribution in a closed system that may be a country or the whole world or a stock exchange. Our main argument is that in such a system interaction of agents is described by nonlinear equations with the conservation of two integrals of motion being total number of agents (norm or total probability analogous to number of system particles) and total wealth (analogous to total system energy). Under these conditions the wealth sharing is described by the universal RJ thermal distribution (2.1) as it is the case for various physical systems [17, 23–25, 27, 54–58]. The striking feature of RJ thermalization (2.1) is that at low system energy (low ε) there is the physical phenomenon of RJ condensation when a high fraction of total probability is located at lowest energy states that corresponds to the high fraction of poor households with very low wealth and also other small fraction of oligarchic households that monopolizes a big fraction of total wealth. Thus according to the WTH phenomenon a huge wealth inequality in the world [37, 38] finds a natural thermodynamic explication. We show that the WTH theory gives a good description of the Lorenz curves of US, UK and the whole world. It also gives a very good description of capitalization of companies at stock exchange of New York, London, Hong Kong demonstrating the universality of RJ thermalization description.

On the basis of WTH theory we see that a reduction of wealth inequality can be realized by an increase of rescaled system energy ($\varepsilon = E/B$). This point is illustrated in Fig. 12 which shows a color plot of the Lorenz curves of the RJE model at $a = 5.34$ for different values ε. For this case there is very good matching with the World 2021 data at $\varepsilon = 0.008553$ as can be seen in Fig. 9 and at larger values of ε the green/red domain with moderate/high wealth increases. The simplest way to reach this is to reduce the global dispersion of wealth (given by B) that can be realized by a high taxation of high wealth revenues.

In the next Part II, we give more justifications for the WTH approach showing that a nonlinear perturbation of social networks leads to the RJ thermalization and condensation.

3 Part II: Dynamical thermalization in social networks

3.1 Prologue II

During last years social networks gained a significant importance for communications, opinion formation and relations analysis in a human society (see e.g. [30, 31]). Many fundamental properties of such networks have been studied with a variety of their applications established

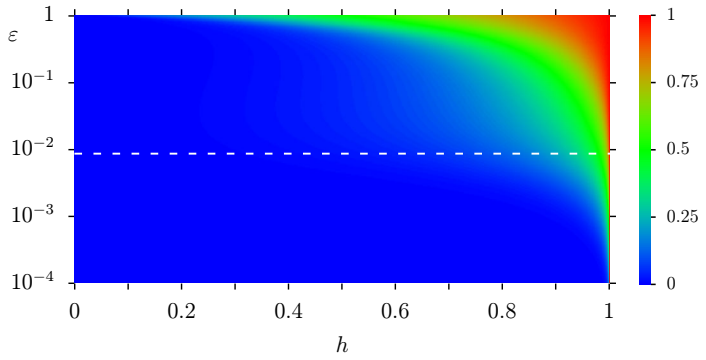

Fig. 12 Color plot of cumulated wealth w from the Lorenz curves of the RJE model (2.2) ($N = 10000$) with the parameter $a = 5.34$. The x-axis corresponds to the fraction of households $h \in [0, 1]$ and the y-axis to the rescaled energy $\varepsilon = E/B \in [10^{-4}, 1[$ in logarithmic representation. The white dashed line corresponds to the value $\varepsilon = 0.008553$ obtained by matching the Gini coefficient of the RJE model (at $a = 5.34$, $N = 10000$) with the data of World 2021 from [38] (see Fig. 9). Note that the color values along the dashed line correspond to the blue RJE curve in Fig. 9

for multiple fields of science. However, all these studies are based on a linear matrix algebra of links between network nodes provided by their adjacency matrix. At the same time it may be interesting and important to analyze the effects of nonlinear interactions between network nodes (agents or users). Indeed, it looks rather natural to assume that in real relations between network agents nonlinear effects should play an important role. With this aim we consider a nonlinear perturbation of a typical example of a nondirected social network which is taken from the database compiled by Newman [65]. It represents a collaboration network of scientists studying networks created by Newman [66–68]. Selected results for a different example network of politicians generated from Facebook with network data of [69] are presented elsewhere [32].

These types of networks are nondirectional so that their adjacency matrix is symmetric and can be viewed as a certain Hamiltonian of a quantum system or a system of coupled linear oscillators. As in [17] a nonlinear interaction is included as a nonlinear frequency shift on a network site (node, agent). The dynamical evolution of the obtained system of nonlinear oscillators has two integrals of motion being the total energy and total norm (probability or number of agents). This corresponds to two integrals of motion in the evolution of wealth of agents considered in [50, 51] assuming that the wealth is associated to the system energy.

We show that above a certain chaos border of nonlinear interactions a dynamical thermalization takes place in the social networks nonlinear dynamical models leading to RJ thermal distribution (2.1). At low values of the total system energy, or total wealth, RJ condensation emerges in the considered social networks leading to an enormous phase of poor households and a small oligarchic fraction capturing a main part of total wealth. Since social networks can be considered as realistic models of relations in a human society the obtained results for dynamical RJ thermalization provide an additional support and justification for the WTH related to the origins of wealth inequality considered in Sect. 2.

In a certain sense the presented studies of dynamical thermalization in social networks can be considered as an extension of the studies of the FPU problem [2] but with a Hamiltonian part of linear oscillators based on a typical structure of social network links. This linear part of the Hamiltonian is similar to that of the random matrix model NLIRM [17]. We attribute this similarity between two systems to the fact that the nodes in social networks are

well connected with each other and only a few link hoppings are required to pass from any node to any other node (see e.g. [30, 31]). Indeed, only 4-5 such link transitions, called the Erdös number, are required to connect any node of the entire Facebook with 8×10^8 users to any other node [70]. Due to this the so called "six degrees of separation" [30, 31], the nonlinear interactions lead to an efficient chaos transition with dynamical thermalization and RJ condensation.

3.2 Model description and numerical methods

In this work, we consider a nondirected network of $N = 379$ known scientists with $N_\ell = 1828$ links from [66, 67], called the *netscience network*, where certain weights are attributed to the links (see Eq. (2) of [66]). Here links $i \to j$ and $j \to i$ for different nodes $j \neq i$ are counted twice in the definition of N_ℓ and self links $i \to i$ are absent.

For this network, we define the adjacency matrix A_{ij} by $A_{ij} = w_{ij}$ if there is a link from node j to i and where w_{ij} is the weight of this link and $A_{ij} = 0$ if there is no link $j \to i$. For nondirected networks this matrix is symmetric and has real eigenvalues. We briefly mention that using this matrix A one can define a stochastic matrix S by normalizing the columns of A where eventual empty columns of A for *dangling nodes* are replaced by $1/N$ entries in S but this does not happen for the netscience network. Then the Google matrix G with elements G_{ij} is defined as $G_{ij} = \alpha S_{ij} + (1-\alpha)/N$ with the damping factor α and its typical value $\alpha = 0.85$. The reason for this is to obtain a unique leading eigenvector of G with eigenvalue $\lambda = 1$, called the *PageRank*, which can be computed efficiently by the power method. However, in the network here also for $\alpha = 1$ there is a unique PageRank with a gap between $\lambda = 1$ and other eigenvalues with $|\lambda| < 1$. We refer to Ref. [74] for a review on the network matrices A, S and G and the PageRank (for the more general case of directed networks) .

We associate to the network a "quantum Hamiltonian" by

$$H = A + \kappa H^{\mathrm{GOE}} \tag{3.1}$$

where κ is a small parameter and H^{GOE} is a random GOE-matrix [18–20] with a semicircle density of states of radius unity (at large $N \gg 1$) which corresponds to random gaussian matrix elements with zero mean and variance $\langle (H^{\mathrm{GOE}}_{n,n'})^2 \rangle = (1 + \delta_{n,n'})/(4(N+1))$. The contribution of κH^{GOE} corresponds to a small static perturbation of the network links which we also expect in real life. In this work, we mainly used one specific random realization of H^{GOE} for a given network of size N but we verified with different realizations that the results do not depend on this choice.

Using the matrix H, we consider the nonlinear oscillator system

$$i \frac{\partial \psi_n(t)}{\partial t} = \sum_{n'=1}^{N} H_{n,n'} \psi_{n'}(t) + \beta |\psi_n(t)|^2 \psi_n(t) \tag{3.2}$$

with complex oscillator amplitudes $\psi_n(t)$ for nodes n where β is the parameter of the nonlinear perturbation. The dynamical system (3.2) has two integrals of motion being the *norm* $\mathcal{N}$ and the *classical energy* $\mathcal{H}$:

$$\mathcal{N} = \sum_n |\psi_n|^2 \quad , \quad \mathcal{H} = \sum_{n,n'} \psi_n^* H_{n,n'} \psi_{n'} + \frac{\beta}{2} \sum_n |\psi_n|^4 \, . \tag{3.3}$$

In fact, the system (3.2) is actually a classical Hamiltonian system with Hamilton function $\mathcal{H}$ if we write $\psi_n = (q_n + ip_n)/\sqrt{2}$ with canonical coordinates q_n and p_n. In this work we fix the norm by $\mathcal{N} = 1$. The case $\mathcal{N} \neq 1$ can be transformed to the case $\mathcal{N} = 1$ by a suitable rescaling of ψ and β.

For $\beta = 0$ this system is simply the time dependent Schrödinger equation for a quantum system with the state $|\psi\rangle = \sum_n \psi_n |n\rangle$ (with $\hbar = 1$). It is useful to diagonalize H by $H\phi^{(m)} = E_m \phi^{(m)}$ with eigenvectors $\phi^{(m)}$ (and components $\phi_n^{(m)}$) and to define amplitudes C_m in eigenmode space by

$$C_m = \sum_n \phi_n^{(m)*} \psi_n \ . \tag{3.4}$$

Here we write more general formulas with the complex conjugate of $\phi_n^{(m)}$ which are also valid for the more general case of complex hermitian matrices H even though in our case H is real symmetric where it is possible to choose real eigenvectors $\phi_n^{(m)} \in \mathbb{R}$. Also we assume that the eigenvectors are orthogonal

$$\sum_n \phi_n^{(\tilde{m})*} \phi_n^{(m)} = \delta_{\tilde{m},m} \tag{3.5}$$

so that the matrix $U_{nm} = \phi_n^{(m)}$, containing the eigenvectors in its columns, is orthogonal (or unitary for complex hermitian H) with the diagonalization identity $H = U \hat{E} U^\dagger$ where $\hat{E}_{\tilde{m},m} = E_m \delta_{\tilde{m},m}$ and the inverse transformation of (3.4) being

$$\psi_n = \sum_m \phi_n^{(m)} C_m \ . \tag{3.6}$$

Using (3.4)-(3.6) one can show that the nonlinear system (3.2) can be rewritten in the eigenmode amplitudes C_m as

$$i \frac{\partial C_m}{\partial t} = E_m C_m + \beta \sum_{m_1,m_2,m_3} Q_{m m_1 m_2 m_3} C_{m_2}^* C_{m_3} C_{m_1} \tag{3.7}$$

with nonlinear transition coefficients

$$Q_{m m_1 m_2 m_3} = \sum_n \phi_n^{(m)*} \phi_n^{(m_1)} \phi_n^{(m_2)*} \phi_n^{(m_3)} \ . \tag{3.8}$$

At $\beta = 0$ the solution of this system is $C_m(t) = e^{-i E_m t} C_m(0)$ and for small values of β there is typically a complicated KAM scenario with a transition to a chaotic region in a large part of the phase space for sufficiently large β.

The two integrals of motion (3.3) can be written in the eigenmode amplitudes C_m as:

$$\mathcal{N} = \sum_m |C_m|^2 \quad , \quad \mathcal{H} = \sum_m E_m |C_m|^2 + \mathcal{H}_{\rm nl} \quad , \tag{3.9}$$

$$\mathcal{H}_{\rm nl} = \frac{\beta}{2} \sum_n |\psi_n|^4 = \frac{\beta}{2} \sum_{m_0,\ldots,m_3} Q_{m_0 m_1 m_2 m_3} C_{m_0}^* C_{m_2}^* C_{m_3} C_{m_1} \ . \tag{3.10}$$

As in [17], we solve the nonlinear system by a symplectic fourth order integrator [71] also known as one of the splitting methods [72, 73]. More details about our implementation of this method can be found in the supplementary material of [17]. This method has the advantage that it respects the symplectic symmetry of the problem. In particular the first integral $\mathcal{N}$ is exactly conserved (up to usual numerical rounding errors) while the second integral $\mathcal{H}$ varies

only slightly in time with a small error $\sim dt^4$ and can be used to verify if the choice of dt is appropriate.

As initial condition, we usually start with an eigenstate located at an initial energy mode m_0 with $C_m(t=0) = \delta_{m,m_0}$. For the netscience network, we also consider a few cases where the initial state is localized on some specific node n_0 with $\psi_n(t=0) = \delta_{n,n_0}$ (i.e. $C_m(t=0) = \phi_{n_0}^{(m)*}$). As in [17] an integration time step dt is chosen in such a way that the second integral of motion $\mathcal{H}$ is conserved with a high relative precision being below 10^{-4} for most initial modes (or $\sim 10^{-2}$ for very few boundary modes; note that due to the method the first integral $\mathcal{N}$ is always conserved "exactly" with numerical precision $\sim 10^{-15}$).

3.3 Theoretical elements of RJ thermalization

At sufficient strong values of β and long times t, we expect the nonlinear system to be chaotic and the amplitudes to be somehow ergodic. Assuming a simple behavior $\psi_n(t) \sim 1/\sqrt{N}$ the typical value of the nonlinear energy contribution in $\mathcal{H}$ is $\mathcal{H}_{\rm nl} \sim \beta/N$ which can be neglected at $N \gg 1$ and then we have:

$$E = \mathcal{H} \approx \sum_m E_m |C_m(t)|^2 \tag{3.11}$$

where E is the specific energy value of the integral $\mathcal{H}$. However, in real systems, such as the network generated matrices H considered here, the assumption $\psi_n(t) \sim 1/\sqrt{N}$ may not be realistic, especially at initial times. More generally, the nonlinear energy contribution is $\mathcal{H}_{\rm nl} = \beta/\xi_{\rm IPR}$ where

$$\xi_{\rm IPR} = \left(\sum_n |\psi_n|^4 \right)^{-1} \tag{3.12}$$

is the *inverse participation ratio* (IPR) on the state ψ_n. The IPR corresponds roughly to the number of populated nodes and is broadly used in the problems of disordered solids (see e.g. [75]). The identity (3.11) is still valid if $\beta/\xi_{\rm IPR}$ can be neglected for sufficiently large values of $\xi_{\rm IPR} \gg \beta$. For the case of the eigenmode initial condition with $\psi_n(t) \approx \phi_n^{(m_0)}$ at small times it is the IPR of the eigenstate $\phi^{(m)}$ which fixes the value of $\mathcal{H}_{\rm nl}$ at initial times. We discuss the IPR for the eigenstates of both models in the next sections pointing out that certain eigenmodes may have relatively small IPR values (depending on E_m and κ).

In any case, even if the initial value of $\mathcal{H}_{\rm nl}$ is not very small, we expect that it decays with time t and that (3.11) holds at large times (assuming a chaotic behavior, i.e. no KAM localized state for very small β). This situation corresponds to a microcanonical ensemble with energy conservation (3.11) and an additional second constraint

$$1 = \mathcal{N} = \sum_m |C_m(t)|^2 \,. \tag{3.13}$$

This special microcanonical ensemble can be treated analytically in a simple way only for small energies (temperatures) with E in the lower part of the spectrum E_m and it is more

convenient to replace it with a grand canonical ensemble with a probability density

$$P(\{C_m\}) = \frac{1}{Z} \exp\left(-\sum_m \frac{E_m - \mu}{T} |C_m|^2 \right) \quad , \tag{3.14}$$

$$Z = \int \prod_m d^2 C_m \exp\left(-\sum_n \frac{E_m - \mu}{T} |C_m|^2 \right)$$
$$= \pi^N \prod_m \frac{T}{E_m - \mu} = \pi^N \prod_m \rho_m \quad \text{with} \quad \rho_m = \langle |C_m|^2 \rangle = \frac{T}{E_m - \mu} \tag{3.15}$$

being the (thermalized) average *occupation probability of the mode m*. Here the temperature T and the chemical potential μ are determined such that both constraints are verified in average:

$$1 = \sum_m \rho_m \quad , \quad E = \sum_m E_m \rho_m \; . \tag{3.16}$$

(See also [17] for more details on this.) The probability density (3.14) corresponds to the RJ thermalization for classical fields. The condition $\rho_m > 0$ (for all m) ensures that there is only a unique physically valid solution of (3.16) with either $T > 0$, $\mu < E_1$ or $T < 0$, $\mu > E_N$.

For the numerical system evolution we compute the time average $\rho_m(t) = \langle |C_m(\tilde{t})|^2 \rangle$ over time intervals $t/2 < \tilde{t} \leq t$ for successive discrete time values $t = 2^l \leq t_{\max}$ with $l = 2, 3, \ldots, l_{\max}$ and $t_{\max}$ being typically $2^{22} - 2^{24}$ for the netscience network. These values for $\rho_m(t)$ can be compared to the thermalized theoretical values $\rho_{m,RJ} = T/(E_m - \mu)$ where T and μ are determined from the constraints (3.16) using the value $E = \langle E \rangle = \sum_m E_m \rho_m(t)$ to fix the energy from the numerically obtained values of $\rho_m(t)$.

Note that for the eigenmode initial condition with $C_m(t = 0) = \delta_{m,m_0}$, we typically have $E \approx E_{m_0}$ if $\mathcal{H}_{\rm nl}(t = 0)$ can be neglected. However, in case of relatively large β values and small IPR, with a significant initial value of $\mathcal{H}_{\rm nl}(t = 0)$, we have the more precise relation $E = E_{m_0} + \mathcal{H}_{\rm nl}(t = 0)$ which may give a significant energy shift in the linear part at larger times scales $\langle E \rangle = \mathcal{H} - \mathcal{H}_{\rm nl}(t) = E - \mathcal{H}_{\rm nl}(t) \approx E = E_{m_0} + \mathcal{H}_{\rm nl}(t = 0)$ assuming that $\mathcal{H}_{\rm nl}(t)$ becomes small for large t (for "ergodic states" in a thermalized regime). However, the initial value $\mathcal{H}_{\rm nl}(t = 0)$ may be rather large such that E_{m_0} and $\langle E \rangle$ are rather different. Therefore, it is more appropriate to use $\langle E \rangle = \sum_m E_m \rho_m(t)$ (with numerical values of $\rho_m(t)$ at large t) rather than E_{m_0} to estimate the value of E to determine T and μ from (3.16) and to compute the theoretical RJ values which are to be compared with the numerical results. We see in the next sections that the numerical data $\rho_m(t)$ indeed approach the thermalized theoretical values for sufficiently large t and the netscience network while for the politician network (studied in [32]) the situation is more difficult due to a limited available integration time.

Another quantity of thermalization is the entropy of the system as a function of either $\langle E \rangle$ or t. There are two points of view to define the entropy. The first one is to use the discrete occupation probabilities ρ_m and define the quantum von Neumann entropy by

$$S_q = -\sum_m \rho_m \ln(\rho_m) \; . \tag{3.17}$$

The latter can also be viewed as the entropy of the associated quantum system of the N levels of the Hamiltonian H with neglected nonlinear term.

The second point of view is based on the underlying classical nonlinear oscillator system with the classical Boltzmann entropy:

$$S_B = -\int \prod_m d^2C_m \; P(\{C_m\}) \ln\left(P(\{C_m\})\, h_B^N\right) \tag{3.18}$$

where $P(\{C_m\})$ is the classical probability density (in some statistical ensemble) of the oscillator amplitudes C_m and h_B is a small constant which compensates the physical dimension in the logarithm. The interpretation of this constant is that we use the discrete probabilities $p(\{C_m\}) = P(\{C_m\})\, h_B^N$ of finding a micro-state in a given elementary cell of volume h_B^N at phase space point $\{C_m\}$ to define the entropy by a sum over a grid of such elementary cells: $-\sum p(\{C_m\}) \ln(p(\{C_m\})$ which gives exactly the above expression (3.18). Below, we give an explicit numerical choice for the parameter h_B which corresponds to a certain constant offset in the definition of S_B.

The formula (3.18) is numerically not convenient since the classical probability density in phase space is not easily available from the trajectory $C_m(t)$ and the integral itself (over many variables) is also difficult to evaluate. In thermal equilibrium, we can replace $P(\{C_m\})$ by (3.14) which gives

$$S_B = \ln(Z/h_B^N) + \sum_m \frac{E_m - \mu}{T} \langle |C_m|^2 \rangle = \ln(Z/h_B^N) + N \tag{3.19}$$

$$= \sum_m \ln\left(\rho_m/h_B\right) + N\,(1 + \ln \pi)\ . \tag{3.20}$$

The expression (3.20) is also more generally valid (outside thermal equilibrium) if we assume independently gaussian distributed amplitudes:

$$P(\{C_m\}) \sim \exp\left(-\sum_m a_m |C_m|^2\right) \tag{3.21}$$

with arbitrary coefficients a_m related to $\rho_m = \langle |C_m|^2 \rangle = 1/a_m$. In thermal equilibrium we have $a_m = (E_m - \mu)/T$ but we may assume that (3.21) is also valid at sufficiently large finite iteration times if $\rho_m = 1/a_m$ is computed as some suitable time average over the trajectory. However, we insist that this assumption is not necessarily very exact especially at small t and that outside thermal equilibrium (3.20) is only a convenient approximation of (3.18) in terms of parameters ρ_m obtained from the numerical procedure.

To have reasonable numerical values of S_B which are (mostly) positive, we choose the numerical value $h_B = 1/N^2$ for the data and figures presented in this work (the numerical choice of h_B defines only a certain constant offset in the definition of S_B). Since typical values of ρ_m are $\sim 1/N$ (at rather larger T) this gives indeed $\rho_m \gg h_B$. In particular for uniform $\rho_m = 1/N$ we have $S_B/N = \ln(N) + 1 + \ln \pi$ which is comparable to $S_q = \ln(N)$. However, at very small times and/or small values of β it is still possible that many values of ρ_m are below $1/N^2$ which gives potentially negative values of S_B. This is an artificial effect of the classical oscillator model and we remind that the entropy of classical systems (oscillators, ideal gas etc.) typically behaves as $S \sim \ln(T)$ for small T with a logarithmic singularity at $T \to 0$. For practical reasons and since S_B is extensive, we consider typically the entropy per mode S_B/N which has comparable numerical values to S_q assuming $\rho_m \sim 1/N$.

We note that in our model the 2nd law of thermodynamics applies to the 2nd entropy S_B and technically it does not apply to S_q. In particular, it is possible that $S_q(t)$ may temporarily decrease with t for certain specific situations (see below) while $S_B(t)$ always increases with

Table 1 Table of node names with largest eigenvector components. The first three columns show names of 10 top nodes in K_m-rank order ($K_m = 1, \ldots, 10$) obtained by ordering the eigenvectors components of modes $m = 1, 2, 3$ of lowest energies E_m with decreasing values of $|\phi_n^{(m)}|$ (in n for given value of m). The 4th (6th) column corresponds to the K-rank order for the PageRank at $\alpha = 1$ ($\alpha = 0.85$) and the 5th column contains the PageRank probabilities (at $\alpha = 1$) for the node list in the 4th column

K_1	K_2	K_3	$K(\alpha = 1)$	$P(\alpha = 1)$	$K(\alpha = 0.85)$
Barabasi	Pastorsatorras	Newman	Barabasi	0.03064	Barabasi
Jeong	Sole	Pastorsatorras	Newman	0.02349	Newman
Albert	Vespignani	Vespignani	Jeong	0.01839	Sole
Oltvai	Newman	Watts	Pastorsatorras	0.01736	Jeong
Ravasz	Valverde	Girvan	Moreno	0.01532	Pastorsatorras
Bianconi	Watts	Moore	Vespignani	0.01532	Boccaletti
Demenezes	Ferrericancho	Stauffer	Sole	0.01532	Vespignani
Dezso	Girvan	Sneppen	Boccaletti	0.01226	Moreno
Vicsek	Montoya	Park	Kurths	0.01124	Kurths
Yook	Moore	Lusseau	Vazquez	0.01124	Stauffer

t (except for a few cases with a very minimal decrease at very short times and/or small values of β below the chaos border). Furthermore, the usual thermodynamic relation $dS/dE = 1/T$ only holds for $S = S_B$ (and not for S_q), that can be verified by a rather simple calculation from (3.20) using $\rho_m = T(E)/(E_m - \mu(E))$. In particular the terms $\sim d\mu(E)/dT$ cancel exactly due to the two constraints (3.16).

3.4 Netscience network model

In this section, we present the results for the netscience network. Note that additional results and figures related to this section are available at [32].

The issue of thermalization depends in a sensitive way on the "ergodic" structure of the eigenvector components $\phi_n^{(m)}$ of the matrix H given in (3.1). We compute the eigenvalues and eigenvectors of this matrix for the netscience network with $N = 379$ for different values of the parameter κ. For certain eigenvectors of modes m with minimal energies E_m, $m = 1, 2, 3, \ldots$, we also determine the ranking index K_m such $|\phi_n^{(m)}|$ is ordered in n in this index, i.e. $|\phi_n^{(m)}| \geq |\phi_{n'}^{(m)}|$ if $K_m(n) < K_m(n')$. The PageRank eigenvector is computed at damping factor $\alpha = 1$ and $\alpha = 0.85$. This is the leading eigenvector of $G(\alpha)$; see text above (3.1) and [74]. Both cases have a similar ranking index K.

In Tab. 1, we present the names of the top 10 nodes for the eigenmodes with $m = 1, 2, 3$ and also both PageRank vectors (at $\alpha = 1$ and $\alpha = 0.85$) ordered by their respective ranking index K_m or $K(\alpha)$. The data in this table was computed for $\kappa = 0$ but the top rankings of the eigenmodes at $\kappa = 0.5$ are actually identical to those of $\kappa = 0$. The top 4 PageRank names at $\alpha = 0.85$ being *Barabasi*, *Newman*, *Sole* and *Jeong* also appear as nodes with strong "community centrality" in [67] (see additional data at Ref. [84] therein). They also play an important role in the PageRank at $\alpha = 1$ with rank values $K = 1, 2, 7, 3$ respectively. *Barabasi* and *Jeong* occupy the positions $K_1 = 1$ and 2 in the first eigenmode ranking for $m = 1$ while *Newman* and *Sole* appear with $K_2 = 4$ and 2 in the 2nd eigenvector. *Newman* also holds the first ranking position $K_3 = 1$ in the 3rd eigenvector. We also mention that each

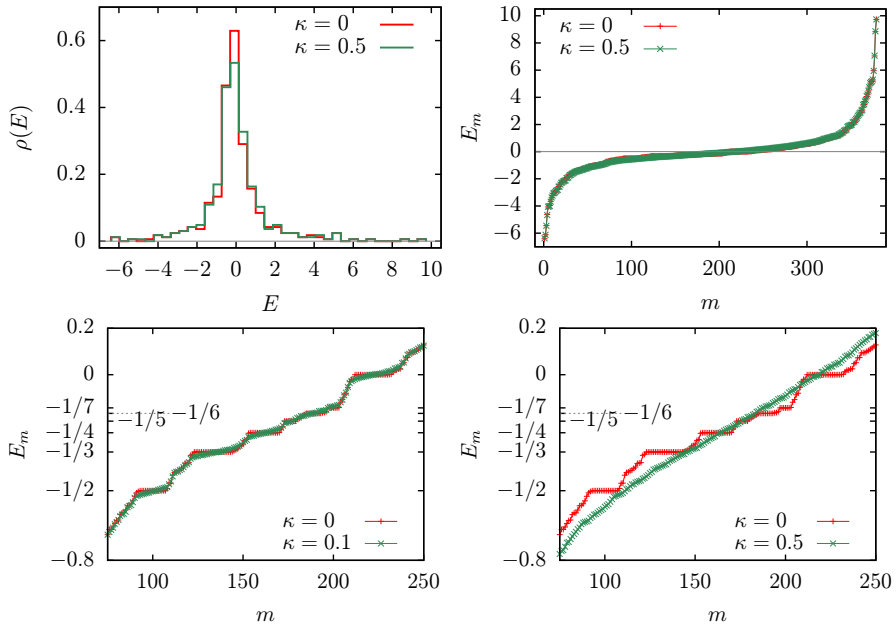

Fig. 13 Spectral properties of the eigenvalue spectrum of the matrix H for the netscience network with $N = 379$ eigenvalues E_m ($E_1 < E_2 < \ldots < E_N$). The top left panel shows the density of states for $\kappa = 0$ and $\kappa = 0.5$ normalized by $\int_{E_1}^{E_N} dE\, \rho(E) = 1$ with histogramm bin width $dE = 10(E_N - E_1)/N \approx 0.436$. The top right panel shows the eigenvalue E_m versus index m for $\kappa = 0$ and $\kappa = 0.5$. Note that $m/N \approx \int_{E_1}^{E_m} dE\, \rho(E)$. Bottom panels show E_m versus m in a zoomed range for either $\kappa = 0$ and $\kappa = 0.1$ (left) or $\kappa = 0$ and $\kappa = 0.5$ (right). The plateau values for $\kappa = 0$ (red data points) at $E_m = 0$ and $E_m = 1/p$ for $p = 2, \ldots, 7$ correspond to degenerate energy levels. Many eigenvectors of these energies (and other energies with nice rational values) have a small support length $l(m) \ll N$ where $l(m)$ is the number of non-zero values of eigenvector components (with numerical precision 10^{-12}). These degeneracies are lifted by small GOE perturbations at $\kappa = 0.1$ or $\kappa = 0.5$. Bottom and top eigenvalues (at $\kappa = 0.5$) are -6.38, -6.12, -5.46, -4.67 and 5.94, 7.06, 8.86, 9.73. (Bottom/top eigenvalues at $\kappa = 0$ are very close)

of the three eigenvectors with modes a $N + 1 - m$ ($m = 1, 2, 3$, $N = 379$) at largest energies (not shown in the table) has actually a rather strong overlap with top nodes with the lowest modes m (e.g. $\phi^{(1)}$ and $\phi^{(379)}$ have some common node names in their top ranking index and similarly for the 2nd and 3rd eigenvectors) while there is no overlap between $m = 1$ and $m = 2$.

Fig. 13 shows in different panels the density of states of H at $\kappa = 0$ and $\kappa = 0.5$ and also the dependence of E_m on m. The global spectral energy band is in the range $E_1 \approx -6.4$ and $E_N \approx 9.7$ (see caption of this figure for 4 bottom and top eigenvalues) with strong gaps of boundary eigenvalues while the density of states has peaked structure around $E = 0$, with a slightly stronger peak for $\kappa = 0$. The global dependence of E_m on m seems rather similar between $\kappa = 0$ and $\kappa = 0.5$ but the zoomed bottom panels show that at $\kappa = 0$ there are several plateau values of degenerate levels at $E = 0$ and $E = -1/p$ for $p = 2, \ldots, 7$ which are lifted by small GOE perturbations. At $\kappa = 0.1$ the degeneracies are only weakly lifted and one can still see the effect of them in the (zoomed) E_m versus m curve while at $\kappa = 0.5$ this curve is essentially a straight line in the shown interval $-0.8 < E_m < 0.2$.

In order to understand these degeneracies we have analyzed the eigenvector structure in more detail by computing for each eigenvector m (at $\kappa = 0$) the *support length* $l(m)$ which we define as the number of nodes n with $\phi_n^{(m)} \neq 0$ (or more precisely with $|\phi_n^{(m)}| > 10^{-12}$ due to the limited numerical precision) and also the IPR (for $\kappa = 0$ and $\kappa = 0.5$).

It turns out that the eigenvectors of the degenerate energies (at $\kappa = 0$) visible in Fig. 13 have small values of the support length in the interval $8 \leq l(m) \leq 48$ ($l(m) = 48$ for $E_m = 0$). There are also other eigenmodes (non degenerate or only with a double degeneracy) with very small support length in the range $2 \leq l(m) \leq 8$. In total there are 104 out of 379 eigenmodes with $l(m) \leq 48$. These modes are all characterized by energies $E_m = p/q$ with nice rational values (maximal $q = 420$ and other $q \leq 12$).

The IPR values of the eigenvectors at $\kappa = 0$ (in the interval $1.77 \leq \xi_{IPR} \leq 45.98$) are actually not strongly correlated to the support length. Globally the IPR is rather small, also for modes with maximal $l(m) = N$, and for some modes with small $l(m)$ the IPR value may be close to $\xi_{\rm IPR} \approx 20$ (about 50% of the possible maximal value).

Globally, the netscience network and its related adjacency matrix has some specific algebraic structure explaining these modes. Even though the netscience network has only one single component of maximal size $N = 379$ there is some hidden subblock structure in some other base obtained by linear combinations of certain states.

We mention, without going into much details, that for $\kappa = 0$ and even strong interaction values such as $\beta = 10$, typical states with initial modes m_0 in the band center do not thermalize well to all modes E_m according to the RJ-values of ρ_m. For many values of m (corresponding to the degenerate modes) the values of ρ_m stay very small even for long times such as $t = 2^{24}$. For this reason, we focus in the following on the case $\kappa = 0.5$ with a rather significant GOE-perturbation which clearly lifts the degeneracies, where all eigenvectors have the maximal value $l(m) = N$ and where the IPR values are roughly a factor 10 larger than for the case $\kappa = 0$. Only a few number of boundary modes, which are clearly in the perturbative regime due to the large gaps, have roughly the same IPR values between $\kappa = 0.5$ and $\kappa = 0$. We assume that it is natural to have in human society a presence of such small random links between society members that can appear due to global information sources (e.g. radio, TV). Thus we present results mainly for the case at relatively small $\kappa = 0.5$ where the RMT perturbation takes out the degeneracies present at $\kappa = 0$.

The values of typical Lyapunov exponents (obtained for initial mode initial conditions), show that at $\beta = 10$ and $\kappa = 0.5$ all modes are in the chaotic regime (see [32]). Even for a very small value of $\beta = 0.2$ the values of Lyapunov exponent is not very small for modes with $-2 < E_{m_0} < 2$ while boundary modes are in the KAM regime. The basic properties of the theoretical thermalized values of ρ_m for the energy spectrum of the netscience network and the energy dependence of temperature T and chemical μ are illustrated in certain figures of [17, 32].

We now turn to the discussion of how well the numerical results for the nonlinear system (3.2) are in agreement with the RJ-theory. As already explained above, we solve (3.2) numerically for the netscience network using initial conditions localized on one energy mode m_0 with $C_m(t = 0) = \delta_{m,m_0}$. Due to the nonlinear term we expect, for sufficiently large values of the parameter β, that the probability states to diffuse approaching to the RJ-distribution. To verify this point, we compute long time averages $\rho_m(t) = \langle |C_m(\tilde{t})|^2 \rangle$ over time intervals $t/2 < \tilde{t} \leq t$ for successive discrete time values $t = 2^l$, $l = 1, 2, \ldots$ with values up to $t = 2^{25}$. Using these numerical averages, we compute S_q and S_B/N using the formulas (3.17) and (3.20) in terms of ρ_m and using $h_B = 1/N^2$ in (3.20). Then we can compare with the theoretical values of S_q and S_B/N using the RJ-thermalized occupation probabili-

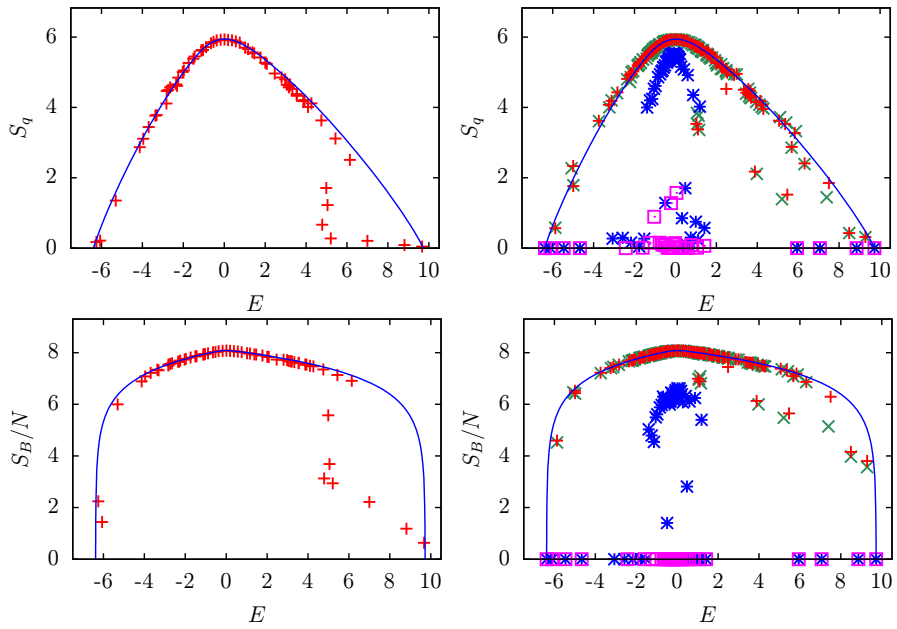

Fig. 14 Entropy S_q (S_B/N) versus energy E in top (bottom) panels for certain cases of the netscience network with $\kappa = 0.5$, $N = 379$. Left panels correspond to 64 selected modes at $\beta = 4$ and $t = 2^{22}$ (red $+$ symbols) and right panels correspond to 128 selected modes at $\beta = 10$, $t = 2^{22}$ (red $+$ symbols), $\beta = 10$, $t = 2^{20}$ (green $\times$ symbols), 64 modes at $\beta = 0.2$, $t = 2^{22}$ (blue $*$ symbols) and 32 modes at $\beta = 0.05$, $t = 2^{22}$ (pink $\square$ symbols) In the right bottom panel the data points with $S_B < 0$ (certain points for $\beta = 0.2$ and all points for $\beta = 0.05$) have been shifted up to $S_B = 0$. The blue line shows the energy dependence of the theoretical thermalized entropy for both entropy quantities. S_q (S_B) has been computed by Equation (3.17) (Equation 3.20 with $h_B = 1/N^2$) using ρ_m values obtained as the time average $\rho_m = \langle |C_m(\tilde{t})|^2 \rangle$ for $t/2 < \tilde{t} \leq t$ (for $t = 2^{22}$ or $t = 2^{20}$ according to the selected data in this Figure)

ties $\rho_{m,RJ} = T/(E_m - \mu)$. To obtain the values of T and μ, we need to solve the implicit equations (3.16) with a given energy value E as parameter. One possible choice for the comparison is $E = E_{m_0}$ where m_0 is the used initial mode of the numerical data. However, it turns out that the agreement between numerical and theoretical values is better if we choose $E = \langle E \rangle = \sum_m E_m \rho_m$ (using the numerical values of ρ_m at a given time t) to solve (3.16) to obtain T, μ and $\rho_{m,RJ}$. Typically, we have $\langle E \rangle \approx E_{m_0}$ but for boundary modes with small initial IPR, and larger initial nonlinear energy contribution, there may be a significant energy shift between E_{m_0} and the final $\langle E \rangle$ value (see also the discussion at the beginning of the last section around Eqs. (3.11)-(3.13)).

Thus Fig. 14 compares the energy dependence of the numerical data of S_q and S_B/N for a selected number of initial modes with the theoretical values (for $E = \langle E \rangle$) for the netscience network at $\kappa = 0.5$ and different values of β. For $\beta = 4$ and $\beta = 10$ at $t = 2^{22}$ the numerical entropy values agree very well with the theoretical curves for $E \leq 4$ (with 2-3 exceptions at $\beta = 10$). Some of the boundary modes at $E > 4$ have very low entropy values which can be explained by the large energy gaps for theses modes which are very stable with respect to the nonlinear perturbation. They have also slightly smaller Lyapunov exponents compared to the modes with E_m in the band center. Furthermore, the effect of the energy shift due to the initial nonlinear energy contribution pushes these modes more to the right boundary for

$\beta > 0$ while boundary modes at the lower part of the spectrum are more pushed to the band center with a reduced chaos border by this effect. For $\beta = 10$ the second set of data with $t = 2^{20}$ is very close to the first set if data at $t = 2^{22}$ (with a few exceptions at $E > 0$) showing that most entropy values are already quite stable for $t \geq 2^{20}$. These results are confirmed for other values $1 \leq \beta \leq 20$ (data not shown in this or other figures here) with the same kind of exceptions for $E > 4$ and for $1 \leq \beta \leq 3$ a few boundary modes at the lower energy border for $E \leq -5$ are not well thermalized as well.

The entropy data for very small coupling constants $\beta = 0.2$ and $\beta = 0.05$ (blue and pink data points in the right panels) are clearly below the theoretical curves. Note that for S_B/N negative values have been artificially shifted up to zero values for a better visibility. This vertical shift concerns some boundary modes (all modes) for $\beta = 0.2$ ($\beta = 0.05$) with rather strong negative values of S_B (using the parameter $h_B = 1/N^2$). However, for $\beta = 0.2$ the entropy values of the center energy modes in the interval $-1.5 < E < 1.5$ are not very far from the theoretical curves and they still continue to increase in time (at largest available time values). Also their Lyapunov exponents are somewhat stronger than those of the boundary modes at same value of β. These results indicate that center modes at $\beta = 0.2$ are already in a "weak" chaotic regime, but with reduced Lyapunov exponent and much larger thermalization time scales, while boundary modes are still in a pertubative KAM regime. For $\beta = 0.05$ the entropy values are very low for all modes, most S_q values are close to zero and only three values are between 1 and 2 which is 1 to 3 times smaller than the theoretical S_q value. We know that in the energy band center there are many oscillators with very close frequencies E_m and in such cases the KAM theory is not valid and even a very small nonlinearity for e.g. 3 oscillators with equal frequencies have about 50% of the phase space being chaotic (see e.g. [76, 77]).

In Fig. 15, we show the dependence of numerical values $\rho_m(t)$ on E_m for the netscience network, $\beta = 10, \kappa = 0.5$, several initial modes m_0 and two time values $t = 2^{22}$ and $t = 2^{24}$ (note that $\rho_m(t) = \langle |C_m(\tilde{t})|^2 \rangle$ for $t/2 < \tilde{t} \leq t$). The blue curve corresponds to the thermalized expression $\rho_{RJ}(E_m) = T/(E_m - \mu)$ with T and μ obtained by solving the implicit equations (3.16) with $E = \langle E \rangle = \sum_m E_m \rho_m(t = 2^{24})$. The states with initial modes $m_0 = 4, 46, 292$ are very well thermalized with values of ρ_m that are in good agreement with the theoretical curve. There are somewhat stronger fluctuations for $m_0 = 292$ and the shorter time value $t = 2^{22}$. Even the first (left) boundary mode $m_0 = 1$ is quite well thermalized while the second mode $m_0 = 2$ is not well thermalized with most ρ_m values below the theoretical curve and a few data points strongly above it. The reason for this strange behavior is that the first mode $m_0 = 1$ has a very strong energy shift effect ($E_1 = -6.38$ while $\langle E \rangle = -4.99$) due to its particularly small value of the initial IPR (≈ 2.8).

The right boundary mode $m_0 = 378$ has a significant nonlinear energy shift being close to maximal possible energy values. Thus the energy integral of motion (energy constraint) does not allow to diffuse to a more ergodic state and the system remains in the integrable KAM regime.

More generally, for modes with $T < 0$ and $E_{m_0} > 0$ the energy shift effect has a tendency to increase the energy to a region with a stronger condensation and due to the energy constraint it is more difficult to thermalize while at $E_{m_0} < 0$ the energy shift effect facilitates thermalization (to a certain modest degree). This can be seen at the modes $m_0 = 1$ and $m_0 = 4$ and also in Fig. 14 where many modes with $E > 4$ do not thermalize and their entropy values are clearly below the theoretical curves (for the cases $\beta = 4$ and $\beta = 10$ with good thermalization at $E < 4$).

Figs. 16 and 17, show the entropy time dependence of of $S_q(t)$ and $S_B(t)/N$ for the 4 well thermalized modes $m_0 = 1, 4, 46, 292$ at $\beta = 10$ (full lines) and also for $m_0 = 4, 46, 292$ at

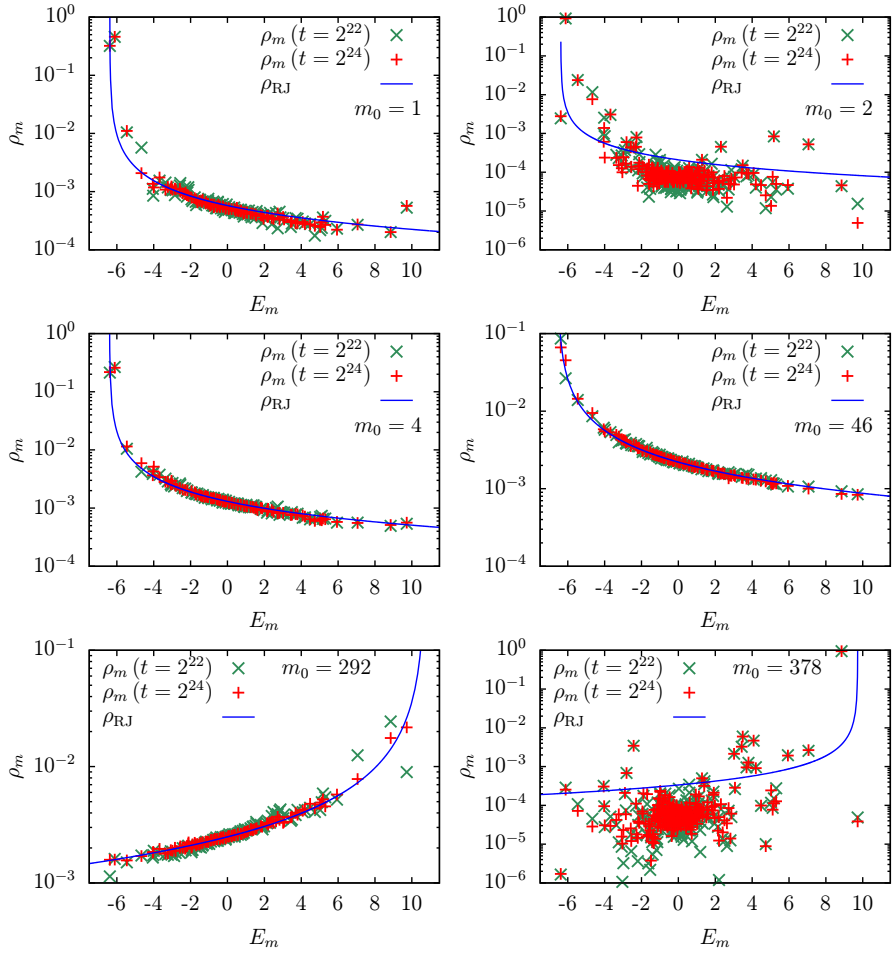

Fig. 15 Dependence of $\rho_m(E_m)$ on E_m for the netscience network with $\kappa = 0.5$, $\beta = 10$, $N = 379$, the initial condition $C_m(t=0) = \delta_{m,m_0}$ where the initial modes are $m_0 = 1, 2, 4, 46, 292, 378$. ρ_m has been obtained as the time average $\rho_m = \langle |C_m(\tilde{t})|^2 \rangle$ for $t/2 < \tilde{t} \leq t$ for $t = 2^{22}$ (green $\times$ symbol) and $t = 2^{24}$ (red $+$ symbol). The blue curve shows the RJ theoretical curve $\rho_{\rm RJ}(E_m) = T/(E_m - \mu)$ with T and μ determined from the implicit equations (3.16) and using the mean linear energy of the state $\langle E \rangle = \sum_m E_m \rho_m (t = 2^{24})$ for the value of E. The values of T, μ and $\langle E \rangle$ for the 6 initial modes $m_0 = 1, 2, 4, 46, 292, 378$ are $T = 0.003689, 0.001347, 0.008348, 0.01443, -0.02676, -0.003266$, $\mu = -6.388, -6.384, -6.402, -6.555, 10.74, 9.729$ and $\langle E \rangle = -4.99, -5.874, -3.238, -1.088, 0.6025, 8.492$. Note that the case of the initial mode $m_0 = 1$ has finally at large times higher values of T, $-\mu$ and $\langle E \rangle$ than the case for $m_0 = 2$ which is due to a stronger energy shift from the nonlinear energy contributions for $m_0 = 1$

$\beta = 0.2$ (dashed lines of same color for corresponding modes). The plateau values correspond to the used intervals for the time average in the computation of $\rho_m(t)$ between $t/2$ and t for $t = 2^l, l = 1, 2, \ldots 24$.

For $\beta = 10$ both entropy quantities increase with time and saturate at values close the theoretical thermalized values (dotted lines). The initial values between $t = 1$ and $t = 2$ are already ~ 1 (for S_q) or ~ 4 (for S_B). Note this figure does not show any data for the very initial time interval $t \in [0, 1[$ with at least 10 (or more) basic integration steps with $dt = 0.1$

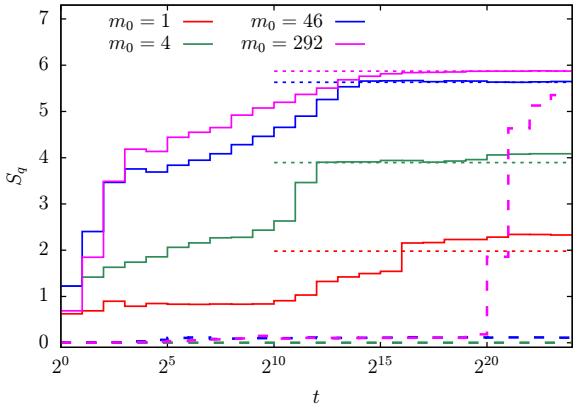

Fig. 16 Time dependence of S_q for the netscience network with $\kappa = 0.5$, $N = 379$. The full lines with colors red, green, blue, pink correspond to $\beta = 10$ for modes $m_0 = 1, 4, 46, 292$ respectively, the dashed lines correspond to $\beta = 0.2$ (for $m_0 = 4, 46, 292$ with colors green, blue, pink) and the dotted lines indicate the theoretical thermalized RJ values. S_q has been computed by (3.17) using $\rho_m(t)$ values obtained as the time average $\rho_m = \langle |C_m(\tilde{t})|^2 \rangle$ for $t/2 < \tilde{t} \leq t$

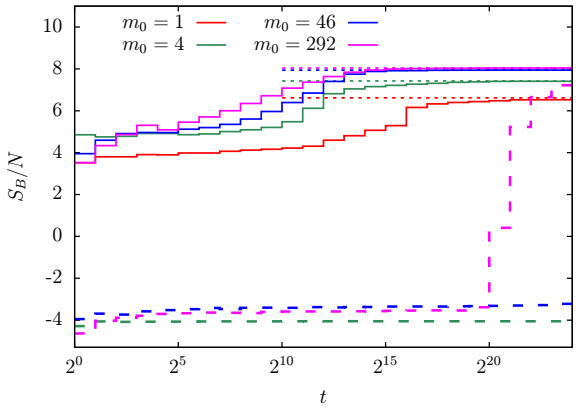

Fig. 17 Time dependence of S_B for the netscience network with $\kappa = 0.5$, $N = 379$. The full lines with colors red, green, blue, pink correspond to $\beta = 10$ for modes $m_0 = 1, 4, 46, 292$ respectively, the dashed lines correspond to $\beta = 0.2$ (for $m_0 = 4, 46, 292$ with colors green, blue, pink) and the dotted lines indicate the theoretical thermalized RJ values. S_B has been computed by (3.20) using $h_B = 1/N^2$ and $\rho_m(t)$ values obtained as the time average $\rho_m = \langle |C_m(\tilde{t})|^2 \rangle$ for $t/2 < \tilde{t} \leq t$

(or less) at which there is already some initial diffusion from $S_q = 0$ (or $S_B = -\infty$) of the mode localized initial condition to some finite values. For S_q (at $\beta = 10$) and the modes $m_0 = 1, 4$ the latest values of $S_q(t)$ are even a bit above the thermalized values. A similar effect for a well thermalized boundary mode was also observed in [17] (for intermediate time scales) and such a behavior is indeed possible since S_q is different from the thermodynamical entropy S_B/N. Furthermore, S_q is not maximal at the thermalized $\rho_{m,RJ} = T/(E_m - \mu)$ values but S_B/N is of course maximal for $\rho_{m,RJ}$ which can be verified by a standard textbook calculation by maximizing (3.17) and (3.20). Mathematically, S_q from (3.17) is maximal at the Gibbs values $\rho_{m,G} = e^{-(E_m-\mu_G)/T_G}$ where the Gibbs temperature T_G and chemical potential μ_G are determined from the implicit equations (3.16) using $\rho_m = \rho_{m,G}$.

For $\beta = 0.2$ the modes $m_0 = 4, 46$ stay localized, even with significant negative values of S_B/N (for the parameter choice $h_B = 1/N^2$) and $S_q \approx 0$. It is likely that there are in the KAM regime. The mode $m = 292$ at $\beta = 0.2$ is very interesting with a very late onset of thermalization at $t \approx 2^{20}$, with a "final" value at $t = 2^{24}$ only slightly below the theoretical value.

We also consider (for $\kappa = 0.5$, $\beta = 1, 4, 10$ and the netscience network) two example states where the initial condition is localized on one specific node n_0 (instead of some eigenmode m_0) with $\psi_n(t = 0) = \delta_{n,n_0}$ (i.e. $C_m(t = 0) = \phi_{n_0}^{(m)*}$) being either *Barabasi* or *Newman* which are the two top PageRank nodes (see also Table 1). For example the time

evolution of both entropy quantities is similar to Figs. 16 and 17 with a good convergence to the theoretical thermalized entropy, now in a regime of negative temperature $T < 0$ since the conserved energy is $E \approx \mathcal{H} \approx \beta/2$. Also the data of $\rho_m(t)$ at large times match very nicely the theoretical thermalized curves.

Finally, the results for dynamical thermalization in the netscience network with nonlinear interactions show that the time evolution is converging to the theoretical RJ distribution for a majority of initial conditions if the system is above a certain chaos border with $\beta > \beta_c$ We estimate that $\beta_c \sim 1$ even if a small chaotic component can survive even below β_c as it as the case in [77]. In the regime of dynamical thermalization the Boltzmann entropy is growing monotonically with time reaching its maximal value in the thermal state in agreement with the Boltzmann H-theorem [1].

We mention, that for comparison, we also studied a larger network for $N = 5908$ politicians via Facebook using data from [69]. We find similar RJ thermalization properties for this model but it requires significantly longer times to reach the steady-state regime due to a larger system size (see [32] for a few selected results of this case).

3.5 Wealth inequality and Lorenz curves

It is interesting to compute Lorenz curves for the specific spectra of the network discussed above. We briefly remind the construction procedure which was introduced in Sect. 2. For a given energy spectrum E_m (e.g. for the netscience network at $\kappa = 0.5$), we first compute a shifted spectrum $\bar{E}_m = E_m - E_1$ such that $\bar{E}_1 = 0$ and other $\bar{E}_m > 0$. Then for a specific value of the energy $\bar{E} = E - E_1$ with $\bar{E}_1 < \bar{E} < \bar{E}_N$ corresponding to the rescaled energy $\varepsilon = (E - E_1)/(E_N - E_1) = \bar{E}/\bar{E}_N$ we compute the RJ thermalized values of T, μ and ρ_m in the usual way (T and ρ_m are not modified by the shift and for μ the same shift as for E_m is applied). In particular, the relation $\bar{E} = \sum_m \bar{E}_m \rho_m$ is verified. Using these values of ρ_m we compute (for $0 \leq m \leq N$) the cumulated household fraction $h(m) = \sum_{i=1}^{m} \rho_i$ and the associated cumulated wealth fraction $w(m) = \sum_{i=1}^{m} (\bar{E}_i/\bar{E})\rho_i$ such that $h(0) = w(0) = 0$, $h(N) = w(N) = 1$ and $h, w \in [0, 1]$. The set of points $(h(m), w(m))$ for $0 \leq m \leq N$ then provides the Lorenz curve.

To characterize the degree of "inequality" one uses the *Gini coefficient* defined as the area between the line $w = h$ (of perfect "equality") and the curve divided over its maximal possible value if $w = 0$ (i.e. $1/2$ for the area of the triangle below the line $w = h$).

Fig. 18 shows for the netscience network a certain number of Lorenz curves for different values of the rescaled system energy ε. The largest used value $\varepsilon = 0.38$ is close to the critical value $\varepsilon_c = 0.39622$ at which the transition from $T > 0$ to $T < 0$ appears. As expected at smaller values of ε the curves describe a strong inequality with a value of G close to 1. Here for $\varepsilon \approx \varepsilon_c$ we have $G \approx 0$ and a curve quite close to the line $w = h$ of perfect equality. This is different from the RJS model (of a uniform spectrum) used in Part I where at $\varepsilon = \varepsilon_c = 1/2$ we have found $w = h^2$. Apart from that, for most curves there is a large interval $h \in [0, h_0]$ where $w(h) = 0$ which is due to the very large energy gaps of the first modes at $m = 1, 2, 3, \ldots$ in comparison to the level spacings of modes in the bulk. For $h > h_0$ the curves increase to the final value $w(h = 1) = 1$ and there are rather close to the straight line between $(h_0, 0)$ and $(1, 1)$.

The results of Fig. 18 show that e.g. at $\varepsilon = 0.15$ the phase of absolutely poor households is approximately 60% of all households while the top 10% of most rich households own approximately 32% of total wealth.

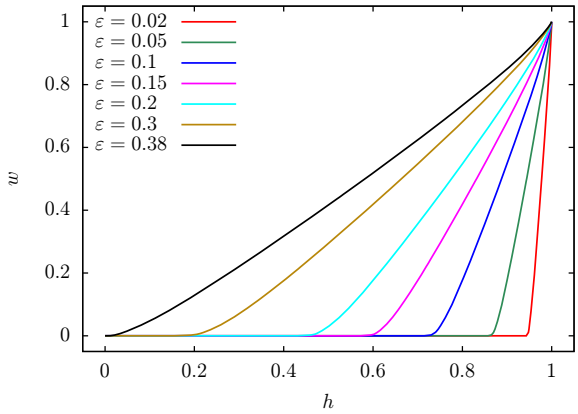

Fig. 18 Lorenz curves for the netscience network with $\kappa = 0.5$, $\beta = 10$, $N = 379$ for different values of the rescaled energy $\varepsilon = (E - E_1)/(E_N - E_1) = \bar{E}/\bar{E}_N$. The x-axis corresponds to the cumulated fraction of households (h) and the y-axis to the cumulated fraction of wealth (w). The largest value $\varepsilon = 0.38$ is slightly below the critical value $\varepsilon_c = 0.39622$ at which the transition from $T > 0$ to $T < 0$ appears. The Gini coefficients G for all curves are $G = 0.9534, 0.8834, 0.7668, 0.5336, 0.6502, 0.301, 0.1321$ (bottom to top)

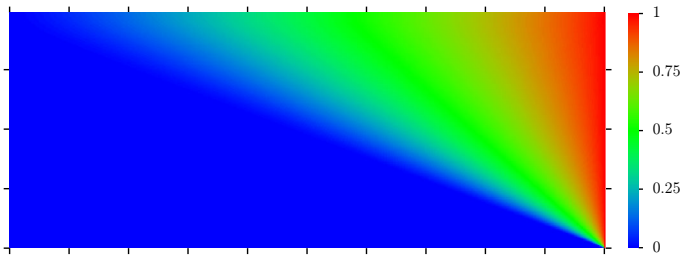

Fig. 19 Color plot of wealth w from Lorenz curves for the netscience network with $\kappa = 0.5$, $\beta = 10$, $N = 379$. The x-axis corresponds to the fraction of households $h \in [0, 1]$ and the y-axis to the rescaled energy $\varepsilon = (E - E_1)/(E_N - E_1) \in [0, \varepsilon_C[$ where $\varepsilon_c = 0.39622$ is the critical value at which the transition from $T > 0$ to $T < 0$ appears. The ticks mark integer multiples of 0.1 for h and ε

Fig. 19 shows a color density plot for the Lorenz curves for a continuous distribution of $\varepsilon \in [0, \varepsilon_c[$ essentially confirming the observations of Fig. 18 the length h_0 of the initial interval (with $w(h) = 0$) behaves roughly as $h_0 \approx \varepsilon/\varepsilon_c$.

The results of this section show that the RJ thermalization and condensation for the netscience network presented in the previous sections leads to the formation of an enormous phase of very poor households and a small fraction of rich households that owns a significant fraction of total system wealth. The presence of a significant energy gap in the energy spectrum of the netscience network enhance the fraction of the poor phase in comparison to the other spectral models considered in Sect. 2. The question of how typical such energy gaps are for social networks requires further studies. Another feature of the considered social network is a strongly peaked density of states approximately at the middle of the energy band. As a result the energies E_m are very flat in this energy region. This is rather different from the RMT model or RJS model of Part I where the density of states is approximately constant in this energy range. We suppose that the origin of this difference is related to the fact that in the considered network we have links between the members of the same society layer or class: scientists linked to scientists, politicians to politicians. Probably this is a general

feature of internet connections where there is little if any distinction between classes of network members. In a real human society there is some kind of natural society stratification: factory workers are mainly linked with workers, peasants with peasants, businessmen with businessmen, aristocrats with aristocrats. This feature is well present in a real human society with its society classes and wealth gradient between classes (of course with fluctuations and relatively weak links between classes). Thus it is possible that the society networks should be revised and updated to include the above feature of human society.

3.6 Overview of social networks results

The presented studies of dynamical thermalization in social networks show that chaos in these systems lead to the RJ thermalized distribution if nonlinear interactions are above a certain chaos border. The time scale for onset of this RJ distribution is determined by the strength of the nonlinearity. This time scale can be relatively long. On a first glance this seems rather surprising in view of a rather small number of links to hope and connect any pair of nodes, with the Erdös number $N_E \approx 4-5$ [30, 31, 70]. However, such link transitions are provided only by the linear part of system Hamiltonian while only the nonlinear interactions lead to transitions between eigenmodes (see (3.7)) with eventual thermalization. Our results show that the RJ thermalization process in the social networks has close similarities with those in the NLIRM model [17]. Thus we expect that the Lyapunov exponents λ_m and the thermalization time scale t_{RJ} have a similar to [17] dependence on nonlinearity β and number of oscillators (nodes) where it was found that the typical Lyapunov exponent values are $\lambda \sim \beta^{1.5}/N^{1.9}$. We expect that $t_{RJ} \propto 1/\lambda$ but further studies are required to confirm these dependencies.

The emergence of RJ condensate leads to a formation of an enormous phase with high fraction of total norm located at low energy, or wealth, states. This leads to a massive fraction of poor households in the social networks as it is well seen in the figures of the Lorenz curves in Sect 3.7. At the same time a significant part of total wealth is captured by a small oligarchic group of rich households. Thus the obtained results for dynamical thermalization in social networks provide a confirmation of WTH origin and highlight the problem of wealth inequality in human society from a new view point.

4 Discussion and conclusion

In 1955 Fermi, Pasta, Ulam and Tsingu performed the first numerical simulations of a chain of nonlinear oscillators with the aim to find a dynamical thermalization and energy equipartition between the degrees of freedom. However, this model happened to have various specific features so that no tendency to equipartition was found in 1955 [2]. To extend these studies a generic model of coupled oscillators was proposed in [17] on the basis of nonlinear perturbation of Random Matrix Theory showing that chaos leads to dynamical thermalization with the resulting RJ distribution over the linear energy eigenmodes. This model has two integrals of motion being the total energy and total norm (probability). Thus the RJ distribution in this isolated Hamiltonian system is characterized by the system temperature $T(E)$ and chemical potential $\mu(E)$.

In fact the emergence of the RJ thermalization had been studied earlier numerically and experimentally for light propagation in multimode optical fibers [26, 53–58], even if the origin of this thermalization was attributed to the Kolmogorov-Zakharov turbulence [25] without links to chaos and KAM integrability. The emergence of RJ condensation was estab-

lished numerically [54] and experimentally [53, 55]. The emergence of an RJ condensate and thermalization in quantum chaos fibers with the nonlinear Schrödinger equation was demonstrated in numerical and analytical studies reported in [27]. At the same time it should be pointed out that the Fröhlich condensate for molecules at room temperature, discussed in [28, 29], has also certain similarities with the RJ condensate, even if in [28, 29] the system is considered under external pumping and dissipation (see discussion in [27]).

In Part I we analyzed the consequences of RJ thermalization and condensation associating system energy and norm, both conserved by time evolution. These quantities are related to the global wealth and the number of interacting households which are also conserved as justified in [50, 51]. The performed analysis shows that this WTH description depicts very well the shape of real Lorenz curves of wealth of households for several countries and the whole world. Also the WTH approach well reproduces the Lorenz curves for the stock exchange markets of New York, London and Hong Kong. To provide more arguments in support of the WTH description we studied in Part II the dynamical thermalization in social networks induced by a nonlinear perturbation. Our results show the emergence of RJ thermalization and condensation in social networks with nonlinear interactions between network agents with the interactions being above a certain chaos border. As in Part I the RJ condensation leads to Lorenz curves with an enormous fraction of poor households and a small fraction which owns a main part of total wealth. On the basis of the results of this work we argue that the WTH description provides new perspectives for the understanding of the nontrivial aspects of the wealth inequality in the world.

Acknowledgements We thank A. D. Chepelianskii and L. Ermann for useful discussions. The authors acknowledge support from the grant ANR France NANOX N° ANR-17-EURE-0009 in the framework of the Programme Investissements d'Avenir (project MTDINA). This work was granted access to the HPC resources of CALMIP (Toulouse) under the allocation 2025-P0110.

Funding Open access funding provided by Université de Toulouse. The authors acknowledge support from the grant ANR France NANOX N° ANR-17-EURE-0009 in the framework of the Programme Investissements d'Avenir (project MTDINA).

Data availability This work uses specific datasets about wealth data for countries, stock market, network data etc. available at Refs. [31, 37–39, 42, 60–69].

Declarations

Conflict of interest The authors declare no conflicts of interest.

References

1. Boltzmann, L.: Weitere Studien über das Wärmegleichgewicht unter Gasmolekülen. Wiener Berichte **66**, 275 (1872)
2. Fermi, E., Pasta, J., Ulam, S.: Studies of non linear problems, Los Alamos Report LA-1940 (1955); published later in E.Fermi *Collected papers*, E.Serge (Ed.) **2**, 491, Univ. Chicago Press, Chicago IL

(1965); see also historical overview in T.Dauxois *Fermi, Pasta, Ulam and a mysterious lady*, Phys. Today **61(1)**, 55 (2008)
3. Zabusky, N.J., Kruskal, M.D.: Interaction of "solitons" in a collisionless plasma and the recurrence of initial states. Phys. Rev. Lett. **15**, 240 (1965)
4. Gardner, C.S., Greene, J.M., Kruskal, M.D., Miura, R.M.: Method for solving the Korteweg - de Vries equation. Phys. Rev. Lett. **19**, 1095 (1967)
5. Zakharov, V.E., Shabat, A.B.: Interaction between solitons in a stable medium. Sov. Phys. JETP **37**(5), 823 (1973)
6. Toda, M.: Studies of a non-linear lattice. Phys. Reports **18**(1), 1 (1975)
7. Benettin, G., Christodoulidi, H., Ponno, A.: The Fermi-Pasta-Ulam problem and its underlying integrable dynamics. J. Stat. Phys. **152**, 195 (2013)
8. Chirikov, B.V., Izrailev, F.M.: Statistical properties of a non-linear string. Sov. Phys. Doklady **11**(1), 30 (1966)
9. Chirikov, B.V., Izrailev, F.M., Tayursky, V.A.: Numerical experiments on statistical behavior of dynamical systems with a few degrees of freedoms. Comp. Comm. Phys. **5**, 11 (1973)
10. Livi, R., Pettini, M., Ruffo, S., Vulpiani, A.: Chaotic behavior in nonlinear Hamiltonian systems and equilibrium statistical mechanics. J. Stat. Phys. **48**, 539 (1987)
11. Shepelyansky, D.L.: Low energy chaos in the Fermi-Pasta-Ulam problem. Nonlinearity **10**, 1331 (1997)
12. Arnold, V., Avez, A.: Ergodic problems of classical mechanics. Benjamin, N.Y. (1968)
13. Cornfeld, I.P., Fomin, S.V., Sinai, Y.G.: Ergodic theory. Springer-Verlag, N.Y. (1982)
14. Chirikov, B.V.: A universal instability of many-dimensional oscillator systems. Phys. Rep. **52**, 263 (1979)
15. Lichtenberg, A., Lieberman, M.: Regular and Chaotic Dynamics. Springer, N.Y. (1992)
16. Gallavotti (Ed.), G.: The Fermi-Pasta-Ulam problem: a status report, Lect. Notes Phys. **728**, Springer, Berlin (2008)
17. Frahm, K.M., Shepelyansky, D.L.: Nonlinear perturbation of Random Matrix Theory. Phys. Rev. Lett. **131**, 077201 (2023)
18. Wigner, E.P.: Random matrices in physics. SIAM Rev. **9**(1), 1 (1967)
19. Mehta, M.L.: Random matrices. Elsvier, Amsterdam (2004)
20. Guhr, T., Müller-Groeling, A., Weidenmüller, H.A.: Random Matrix Theories in quantum physics: common concepts. Phys. Rep. **299**, 189 (1998)
21. Bohigas, O., Giannoni, M.-J., Schmit, C.: Characterization of chaotic quantum spectra and universality of level fluctuation laws. Phys. Rev. Lett. **52**, 1 (1984)
22. Haake, F.: Quantum signatures of chaos. Springer, Berlin (2010)
23. Landau, L.D., Lifshitz, E.M.: Statistical physics. Wiley, New York (1976)
24. Mayer, J.E., Goeppert-Mayer, M.: Statistical mechanics. John Wiley & Sons, N.Y. (1977)
25. Zakharov, V.E., L'vov, V.S., Falkovich, G.: Kolmogorov spectra of turbulence I, Springer, Berlin, (1992)
26. Picozzi, A., Garnier, J., Hansson, T., Suret, P., Randoux, S., Millot, G., Christodoulides, D.N.: Optical wave turbulence: Towards a unified nonequilibrium thermodynamic formulation of statistical nonlinear optics. Phys. Reports **542**, 1 (2014)
27. Ermann, L., Chepelianskii, A.D., Shepelyansky, D.L.: Dynamical thermalization, Rayleigh-Jeans condensate, vortexes and wave collapse in quantum chaos fibers and fluid of light. J. Phys. A: Math. Theor. **59**, 055702 (2026)
28. Fröhlich, H.: Bose condensation of strongly excited longitudinal electric modes, Phys. Lett. A **26A(9)**, 402 (1968)
29. Fröhlich, H.: Long-range coherence and energy storage in biological systems, Int. J. Quantum Chemistry **II**, 641 (1968)
30. Dorogovtsev, S.: Lectures in Complex Networks. Oxford University Press, UK (2010)
31. Newman, M.: Networks. Oxford University Press, UK (2018)
32. Frahm, K.M., Shepelyansky, D.L.: Wealth thermalization hypothesis and social networks, arXiv:2506.17720 [cond-mat.stat-mech] (2025)
33. Frahm, K.M., Shepelyansky, D.L.: Thermodynamic description of world GDP distribution over countries, arXiv:2512.06420 [cond-mat.stat-mech] (2025)
34. Szavits-Nossan, J., Evans, M.R., Majumdar, S.N.: Constraint driven condensation in large fluctuations of linear statistics. Phys. Rev. Lett. **112**, 020602 (2014)
35. Evans, M.R., Majumdar, S.N., Pagonabarraga, I., Trizac, E.: Condensation transition in polydisperse hard rods. J. Chem. Phys. **132**, 014102 (2010)
36. Filiasi, M., Livan, G., Marsili, M., Peressi, M., Vesselli, E., Zarinelli, E.:*On the concentration of large deviations for fat tailed distributions, with application to financial data*, J. Stat. Mech. P09030 (2014)
37. Piketty, T.: Capital in the Twenty-First Century. Belknap Press of Harvard University Press, Cambridge, MA (2014)

38. Chancel, L., Piketty, T., Saez, E., Zucman, G., et al.:*World Inequality Report 2022*, World Inequality Lab https://wir2022.wid.world (Accessed on 8 June 2025)
39. Roach, B., Rajkanikar, P. J., Goodwin, N., Harris, J.: *Social and Economic Inequality*, An ECI Teaching Module on Social and Environmental Issues, Economics in Context Initiative, Global Development Policy Center, Boston University (2023), https://www.bu.edu/eci/files/2023/05/Inequality-Module-2023.pdf (Accessed 8 June 2025)
40. Lorenz, M.O.: *Methods of measuring the concentration of wealth*, Quarterly Publications of the American Statistical Association, **9**, (New Series, No. 70), 209–219 (1905); https://doi.org/10.1080/15225437.1905.10503443 (Accessed 8 June 2025)
41. Gini, C.: *Sulla misura della concentrazione e della variabilit'a dei caratteri*, Atti del Reale Istituto Veneto di Scienze, Lettere ed Arti, **73**, 1203–1248 (1914), English translation in Metron - Int. J. Statisrics, **63**, 3–38 (2005) https://www.dss.uniroma1.it/RePec/mtn/articoli/2005-1-1.pdf (Accessed 8 June 2025)
42. Wikipedia, *List of sovereign states by wealth inequality*, (Accessed 8 June 2025)
43. Lifshitz, E.M., Pitaevskii, L.P.: *Physical kinetics*, Pergamon Press N.Y. (1995)
44. Angle, J.: The surplus theory of social stratification and the size distribution of personal Wealth. Soc. Forces **65**, 293 (1986)
45. Ispolatov, S., Krapivsky, P.L., Redner, S.: Wealth distributions in asset exchange models. Eur. Phys. J. B **2**, 267 (1998)
46. Dragulescu, A., Yakovenko, V.: Statistical mechanics of money. Eur. Phys. J. B **17**, 723 (2000)
47. Bouchaud, J.-P., Mezard, M.: Wealth condensation in a simple model of economy. Physica A **282**, 536 (2000)
48. Yakovenko, V.M., Rosser, J.B.: Colloquium: Statistical mechanics of money, wealth, and income. Rev. Mod. Phys. **81**, 1703 (2009)
49. Chakrabarti, B.K., Chakraborti, A., Chakravarty, S.R., Chatterjee, A.: Econophysics of income and wealth distributions. Cambridge University Press, N.Y. (2013)
50. Boghosian, B.M., Devitt-Lee, A., Johnson, M., Li, J., Marcq, J.A., Wang, H.: Oligarchy as a phase transition: the effect of wealth-attained advantage in a Fokker–Planck description of asset exchange. Physica A **476**, 15 (2017)
51. Boghosian, B. M.: The inescapable casino, Sci. American, November, 71 (2019)
52. Von Bibow, N. V., Perotti, J.L.: *Study of the Extended Yard Sale model of wealth distribution on Erdos-Renyi random networks*, arXiv:2505.04032[cond-mat.stat-mech] (2025)
53. Krupa, K., Tonello, A., Barthelemy, A., Shalaby, B.M., Bendahmane, A., Millot, G., Wabnitz, S.: Observation of geometric parametric instability induced by the periodic spatial self-imaging of multimode waves. Phys. Rev. Lett. **116**, 183901 (2016)
54. Connaughton, C., Josserand, C., Picozzi, A., Pomeau, Y., Rica, S.: Condensation of classical nonlinear waves. Phys. Rev. Lett. **95**, 263901 (2005)
55. Baudin, K., Fusaro, A., Krupa, K., Garnier, J., Rica, S., Millot, G., Picozzi, A.: Classical Rayleigh-Jeans condensation of light waves: observation and thermodynamic characterization. Phys. Rev. Lett. **125**, 244101 (2020)
56. Podivilov, E.V., Mangini, F., Sidelnikov, O.S., Ferraro, M., Gervaziev, M., Kharenko, D.S., Zitelli, M., Fedoruk, M.P., Babin, S.A., Wabnitz, S.: Thermalization of orbital angular momentum beams in multimode optical fibers. Phys. Rev. Lett. **128**, 243901 (2022)
57. Pourbeyram, H., Sidorenko, P., Wu, F.O., Bender, N., Wright, L., Christodoulides, D.N., Wise, F.: Direct observations of thermalization to a Rayleigh–Jeans distribution in multimode optical fibres. Nature Phys. **18**, 685 (2022)
58. Baudi, K., Garnier, J., Fusaro, A., Berti, N., Michel, C., Krupa, K., Millot, G., Picozzi, A.: *Observation of light thermalization to negative-temperature Rayleigh-Jeans equilibrium states in multimode optical fibers*, Phys. Rev. Lett. **130**, 063801 (2023)
59. Aladangady, A., Forde, A.: *Wealth Inequality and the Racial Wealth Gap*, FEDS Notes Oct 22 (2021) https://www.federalreserve.gov/econres/notes/feds-notes/2021-index.htm, (Accessed 8 June 2025)
60. Chamberlain, E.: *Wealth in Great Britain Wave 4. Chapter 2: Total wealth, Wealth in Great Britain, 2012 to 2014*, 18 Dec 2015https://www.ons.gov.uk/peoplepopulationandcommunity/personalandhouseholdfinances/incomeandwealth/compendium/wealthingreatbritainwave4/2012to2014/chapter2totalwealthwealthingreatbritain2012to2014 (Accessed 8 June 2025)
61. Cowell, F., Nolan, B., Olivera, J., Van Kerm, Ph.: *Wealth, Top Incomes and Inequality*, p.175, in *National Wealth*, Eds. K. Hamilton, and C. Herburn, Oxford Univ. Press, Oxford UK (2017)
62. Holdings SPDR S&P500 ETF Trust of June 16 (2025) https://www.ssga.com/us/en/intermediary/etfs/spdr-sp-500-etf-trust-spy
63. London stock exchange data of capitalization of companies, December 31 (2024) https://www.londonstockexchange.com/reports?trkcode=lsehomstats&tab=issuers (Accessed 19 June 2025)

64. Kong, H.: stock exchange data of capitalization of companies, June 19 (2025) https://www.hkex.com.hk/Market-Data/Securities-Prices/Equities?sc_lang=en (Accessed 19 June 2025)
65. Newman, M. E. J.: *Network data*, http://www.umich.edu/~mejn/netdata, (Accessed 12 September 2025)
66. Newman, M. E. J.: *Scientific collaboration networks. II. Shortest paths, weighted networks, and centrality*, Phys. Rev. E **64**, 016132 (2001)
67. Newman, M.E.J.: Finding community structure in networks using the eigenvectors of matrices. Phys. Rev. E **74**, 036104 (2006)
68. Newman, M. E. J.: *Community Centrality*, http://www.umich.edu/~mejn/centrality (Accessed 12 September 2025)
69. Rozemberczki, B., Davies, R., Sarkar, R., Sutton, C.: *Graph Embedding with Self Clustering*, *GEMSEC: graph embedding with self clustering*, ASONAM '19: Proceedings of the 2019 IEEE/ACM International Conference on Advances in Social Networks Analysis and Mining, page 65, (2020), arXiv:1802.03997 https://doi.org/10.1145/3341161.3342890 (2018)
70. Backstrom, L., Boldi, P., Rosa, M., Ugander, J., Vigna, S.: *Four degrees of separation*, WebSci 2012: Proceedings of the 4th Annual ACM Web Science Conf., pafe 33, https://doi.org/10.1145/2380718.2380723
71. Forest, E., Ruth, R.D.: *Fourth-order symplectic integration*. Physica D. 43: 105 (1990) https://cloudfront.escholarship.org/dist/prd/content/qt35h9v2k9/qt35h9v2k9.pdf (Accessed Dec 2022)
72. McLachlan, R.I., Quispel, G.R.W.: Splitting methods. Acta Numer **11**, 341–434 (2002)
73. MacNamara, S., Strang, G.: *Operator splitting*/ In: R. Glowinski, S. Osher, W. Yin (Eds) *Splitting methods in Communication, Imaging, Science, and Engineering*, Scientific Computation. Springer, Cham. pp.95-114 (2016); https://doi.org/10.1007/978-3-319-41589-5_3
74. Ermann, L., Frahm, K.M., Shepelyansky, D.L.: Google matrix analysis of directed networks. Rev. Mod. Phys. **87**, 1261 (2015)
75. Evers, F., Mirlin, A.D.: Anderson transitions. Rev. Mod. Phys. **80**, 1355 (2008)
76. Chirikov, B.V., Shepelyanskii, D.L.: Dynamics of some homogeneous models of classical Yang-Mills fields. Sov. J. Nucl. Phys. **36**(6), 908 (1982)
77. Mulansky, M., Ahnert, K., Pikovsky, A., Shepelyansky, D.L.: Strong and weak chaos in weakly nonintegrable many-body Hamiltonian systems. J. Stat. Phys. **145**, 1256 (2011)